Characterisation of mesoscale eddies generated in the coastal upwelling region of the tropical northeast Atlantic

Master-Arbeit

im **Masterstudiengang (M.Sc.) Climate Physics**

der Mathematisch-Naturwissenschaftlichen Fakultät

der Christian-Albrechts-Universität zu Kiel

vorgelegt von

Florian Schütte

898872

Erstgutachter: Prof. Dr. rer. Nat. Peter Brandt

Zweitgutachter: Priv.-Doz. Dr. Arne Biastoch

Kiel im Januar 2013

Abstract

The region of the tropical northeast Atlantic (between 12°N - 22°N and 15°W - 26°W) is examined and characterised with regard to mesoscale variability. At first different single eddy events are analysed with the help of different data sets, which were recorded in the region of interest, between the years 2000 and 2011. Of particular interest are the vertical structure, the kinematic properties and the changes during the lifetime of an eddy. Observed eddies had length scales between 30km to 110km and were detectable in time scales of a few days up to nine months. The vertical structures of the velocity field within the eddies varied between high and low baroclinic modes. Surface intensified eddies and eddies, with their core beneath the surface, could be distinguished. Generally, eddies were observed to transport South Atlantic Central Water over the Cap Verde Frontal Zone into a region where North Atlantic Central Water dominates.

Following an exemplary eddy during its lifetime, an enclosed system was observed, which captured South Atlantic Central Water from its place of origin in the upwelling region off Mauretania and suffered almost no lateral mixing on its westward way. Changes that occurred during the lifetime of this eddy were a decrease in the oxygen content, a loss of vorticity, of Eddy Kinetic Energy, of rotation velocity, a deepening of the eddy core and a pulsation (contraction and expansion) of the radius with a periodicity of ~14 days.

In addition, this study concentrates on classifying mesoscale processes within the area of the tropical northeast Atlantic. In order to study the general eddy characteristics and activity, the generating mechanisms, the location of their origin and their pathways, a Sea-Level-Anomaly based Eddie-Tracking-Algorithm was adapted from the Okubo-Weiß method. On a daily average mesoscale structures cover ~15 % of the tropical northeast Atlantic and ~17 ±5 eddies per year are produced in the upwelling region between Senegal and Mauretania. A majority of the observed eddies were topographically generated near the headlands of the coast by instabilities of the near coastal current. Cyclones are produced during boreal winter, especially in January, due to the effect of instabilities from a wind induced southward boundary current, combined with its vertical shear. Anticyclones are generated during late boreal summer due to instabilities of a strong northward boundary current, which can be set in connection with coastal waves. After their generation all eddies travel westwards along distinct corridors with a small polarity depending meridional deflection (anticyclones – equatorward, cyclones - poleward).

Zusammenfassung

Studiert wurde der tropische Nordostatlantik (zwischen 12°N - 22°N und 15°W - 26°W) in Hinblick auf mesoskalige Variabilität. Einzelne Wirbelereignisse wurden mit Hilfe von mehreren Datensätzen, die zwischen den Jahren 2000 und 2011 in der Region erhoben wurden, analysiert. Das Hauptinteresse lag auf der vertikalen Struktur, den kinematischen Eigenschaften und der Veränderung eines Wirbels während seiner Lebenszeit. Betrachtete Wirbel besaßen Längenskalen zwischen 30km und 110km und Zeitskalen zwischen einem Tag und neun Monaten. Vertikale Geschwindigkeitsstrukturen von schwach bis stark barokline, sowie Wirbel mit maximaler Rotationsgeschwindigkeit an und unterhalb der Oberfläche wurden beobachtet. Alle beobachteten Wirbel waren isolierte Systeme, die auf ihrem Wegen nach Westen kaum laterale Einmischung erfuhren. Generell wurde ein Transport durch die Wirbel von südatlantischem Zentralwasser aus den Upwelling-Gebiet vor der mauretanischen Küste, über die Kap Verden Front in eine von nordatlantisches Zentralwasser dominierte Region, beobachtet. Die Veränderungen eines Wirbels während seiner Lebenszeit sind ein Absinken des Sauerstoffgehaltes unter der Grenzschicht, eine Abschwächung der Wirbelbewegung, ein Verlust von kinetischer Energie, ein Absinken des Wirbelkerns und ein Pulsieren des Radius mit einer Periodizität von ~14 Tagen.

Ebenfalls Gegenstand dieser Arbeit ist eine Klassifizierung mesoskaliger Prozesse im tropischen Nordostatlantik im Hinblick auf die generelle Wirbelaktivität, die Lokalisation der Wirbelursprünge, die Mechanismen die Wirbel verursachen und deren Ausbreitung. Zu diesem Zweck wurde ein SLA-Daten basierter Eddie-Tracking-Algorithmus (nach Okubo-Weiß) verwendet. Ein Ergebnis ist, dass durchschnittlich ~15% des tropischen Nordostatlantik von mesoskaliger Variabilität bedeckt sind. Ungefähr 17 ±5 Wirbel pro Jahr bilden sich im Mittel in dem Upwelling-Gebiet zwischen dem Senegal und Mauretanien. Ein Großteil von ihnen sind Ursrung von Instabilitäten des küstennahen Stromes und daher topographisch in der Nähe von Landzungen erzeugt. Wärend des borealen Winters, speziell in Januar, bilden sich hauptsächlich Zyklone, was durch Instabilitäten eines Wind erzeugten südwärtigen Grenzstrom in Kombination mit seiner vertikalen Scherung erklärt werden kann. Antizyklone werden im borealen Sommer durch Instabilitäten eines starken nordwärtigen Grenzstroms erzeugt, der in Beziehung mit einer Küsten-Kelvin-Welle gesehen werden kann. Nach ihrer Entstehung propagieren alle Wirbel in eindeutigen Korridoren nach Westen, mit einer leichten von ihrer Polarität abhängigen, meridionalen Ablenkung (Antizyklone – zum Äquator, Zyklone - zum Pol).

Contents

Page

1. Introduction

The ocean and the atmosphere are fundamentally turbulent systems. Both consist of many different forms of variability on all time and length scales. This work will explain and characterise some forms of variability in the region of the tropical northeast Atlantic (12 °N - 22 °N and 15 °W - 26 °W). To successful accomplish this task it is necessary to classify forms of turbulence and introduce some terms of fluid dynamics. In addition, it is important to get a precise knowledge of the circulation pattern within the selected area.

1.1 Turbulence in the ocean

In the ocean different forms of variability are distinguishable: Firstly, the large scale variations are for example basin and gyre scale variations and large scale waves. Then the so-called mesoscale variability dominates the main ocean circulation through isolated vortexes, small scale waves, jets, meandering currents and fronts. One definition of mesoscale variability is everything corresponding to ocean signals with scales of 50-500 km in space and 10-100 days in time [Marrow and Le Traon (2007)]. The smallest kinds of variability are the submesoscale ocean processes or filaments, they surround mesoscale variability and have space and time scales smaller than 30 km and 10 days. In this work the main focus is set on the study of the mesoscale variability.

Before the satellite era began in the 1970s only using measurements carried out by research ships or moorings, it was difficult to understand the importance and the extent of the mesoscale processes in the world's oceans, due to their high spatial and temporal variability. In the following decades satellites have been able to provide for the first time a global, high-resolution, regular monitoring of the world oceans and show that mesoscale processes are ubiquitous in the world's oceans. These processes are an important component of the dynamic oceanography for all scales, transporting properties such as motion, heat, mass, energy, and a large variety of chemical and biological properties.

The mesoscale variability will be studied in the area of the northeast tropical Atlantic which is defined between 0-20°N and 30°W- 10°W in front of the North African coast. This area includes the eastern boundary upwelling system of the North Atlantic. This wind enhanced coastal upwelling brings cold, nutrient-rich water from deeper layers of the ocean to the surface and thus favours an area of high biological productivity. To emphasize this as an example the two eastern upwelling systems in the Atlantic, in front of Mauretania (north) and

Angola (south), and the two eastern upwelling systems in the Pacific, in front of California (north) and Peru (south), cover 1% of the worlds ocean and are responsible for 20% of the global fish catch [Gruber et al. (2011)].

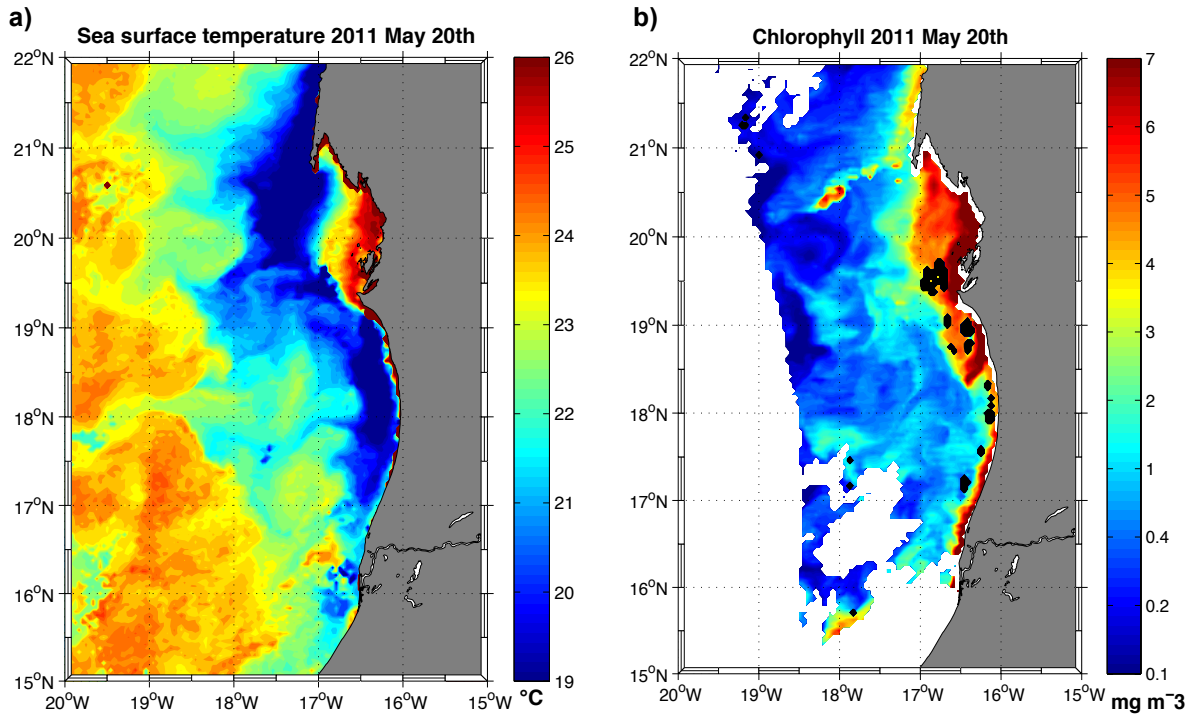

Figure1: Example for the ubiquitous of mesoscale variability and **a)** the sea surface temperature, indicates the upwelling and **b)** chlorophyll concentration, indicates the high biological productivity within the region.

Figure 1 shows the sea surface temperature (SST) and chlorophyll (Chl) in the region of interest, the tropical northeast Atlantic in front of Mauretania. The coastal upwelling area is obvious through the cold waters and the high concentrations in chlorophyll due to the input of nutrient-rich waters at the shelf. This introduces gradients with regard to the surrounding water masses, which allows us to see the mesoscale processes. These are represented in the vortexes and tongues, which tend to dissolve the existing gradients, and transport nutrient-rich water masses from their generating places into the oligotrophic ocean. There appears to be no obvious patterns to it.

The aim of this work is to characterise the mesoscale variability of the tropical northeast Atlantic with regard to the different variability structures, their expansion and their generating mechanisms.

1.2 Scientific importance of this work

An important part of this work is to analyse different single eddy events with the help of different data sets, which were recorded in this region, between 2000 and 2011. In particular, the vertical structure, the kinematic properties and the changes during the lifetime of an eddy will be studied. The result should partly build upon previous studies by combining the techniques of for e.g. Rossby et al. (2011), who explore in detail the dynamics of two coherent eddies in the Caribbean Sea and the work of Chaigneau et al. (2011), who investigate the vertical temperature and salinity structure of mesoscale eddies in the eastern upwelling system off Peru. The aim is to get a precise knowledge of the properties and structures within a general eddy in the tropical northeast Atlantic. From an unique opportunity, an investigation of the development of an eddy during its lifetime can be made, to complete the understanding of single eddy events.

Additionally this study concentrates on the classification of mesoscale processes within the area of the tropical northeast Atlantic to set single eddy events in a bigger context. In regard to this the general dynamics, the general eddy activity and characteristics within the region, the location of their origin, their generating mechanism and pathways will be studied.

Sangrá et al. (2009) examine the eastern subtropical Atlantic, they define the "Canary Eddy Corridor" in which eddies, that are produced from the flow perturbation of the Canary Current and the trade winds at the Canary Islands, mainly propagate. But the tropical northeast Atlantic has never been studied in such a way. Chelton et al. (2007) and Chelton et al. (2011) show global observations of mesoscale variability in the world oceans, where the tropical northeast Atlantic stands out with a low activity of mesoscale variability. This does not seem to be consistent with the data recorded by the GEOMAR in the region between 2000 and 2011, where a lot of mesoscale variability is detected.

In the last decades it has become evident that a better understanding of the large scale circulation requires observations on high temporal and special resolutions to get a better understanding of the small scale variability and its role on climate. Specifically in climate models it stands out that badly represented small scale processes caused by an incorrect or incomplete parameterisation, can lead to major errors. This occurs due to a lack of knowledge about small scale processes in the ocean.

The area off the west coast of Africa with its coastal upwelling and the presence of a pronounced Oxygen-Minimum Zone (OMZ) is particularly of interest concerning the

transport of mass, energy, heat and biological properties (including nutrients, chlorophyll and oxygen) from the shelf into the open ocean.

As mentioned before, it is necessary to first establish the physical background of the mesoscale variability from especially vortexes, the so-called eddies. This is done in chapter *1.3 Physical background*. After that the work contains a section on the region of the northeast tropical Atlantic, with regard to the circulation and the water mass properties and their distribution, *Chapter 1.4*, *1.5* and *1.6*. It is necessary to get a good overview of the circulation of the area, especially with regard to possible sources of instability of the currents within the area, as this could be an indication of possible generating places of mesoscale variability. After that, in *Chapter 2*, the data is described with which the mesoscale variability is detected and studied. *Chapter 3* details the methods with which the data is processed. The results of the work are given in *Chapter 4*. First single eddy events are discussed and then the general view of the whole area, with information about the location of the places of origin of eddies, their expansion and overall activity. *Chapter 5* includes an interpretation of the results and sites them in the context of the current scientific debate. At the end *Chapter 7* summarized the results of the work and gives a perspective on further research.

1.3 Physical background

The velocities in the ocean can be split into two parts, the large scale flow and the small scale turbulence,

$$U = \bar{u} + u' \qquad (1)$$

Eddies which will be discussed here, belong to the second part of the equation, and their kinetic energy is described with the so called Eddy Kinetic Energy (EKE), which is defined as follows:

$$EKE = \frac{1}{2} \cdot (u'^2 + v'^2) \qquad (2)$$

This describes the kinetic energy of the turbulence in the ocean; it can be generated through baroclinic and barotropic instability (Figure 2). If energy is drawn from the mean flow field, e.g. the mean kinetic energy reservoir due to a horizontal shear, the resulting turbulence is called barotropic instability, which generates barotropic eddy structures. Whereas if the energy is drawn from the available potential energy in the ocean, due to a vertical shear in the velocities, this generates baroclinic instabilities and baroclinic eddy stuctures [referred to Holton's (1979) textbook].

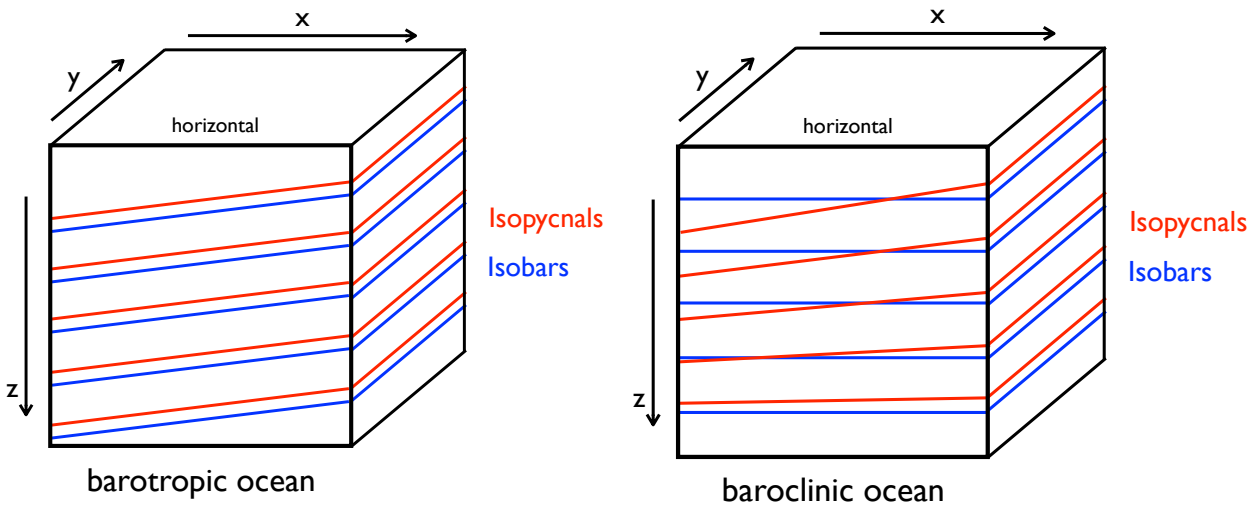

Figure 2: Example for a barotropic and baroclinc ocean. Red lines indicate isopycnals and blue lines isobars.

EKE tends to be greatest where we have strong mean circulation patterns or fronts, there eddies draw energy from the mean kinetic energy field.

Another forcing mechanism which introduces EKE are fluctuating winds, introducing a vertical shear in the flow field, this is particularly important in regions with a weaker mean flow field [Frankignoul and Müller (1979)].

After the eddies are generated, they dissipate through processes involving internal friction and partly feed energy and momentum back into the mean flow. The dissipation rate of an eddy

depends its size relative to the ambient Rossby radius of deformation. If a disturbance is smaller than the ambient Rossby radius of deformation it is more likely to dissipate. The Rossby radius of deformation is defined as:

$$R_d = \frac{c_0}{f} \tag{3}$$

where c_0 is the phase speed of an internal gravity wave and f is the Coriolis parameter. It defines for which horizontal length scale of a fluid motion the effect of the earth's rotation must be taken into account. The scale of mesoscale variability can also be described as the order of the first baroclinic Rossby radius of deformation or internal Rossby radius of deformation [Gill (1982)]. In the area of interest the first baroclinic Rossby radius of deformation is in the order of 40km [Chelton et al. (1998)].

The relative vorticity is also an important term to describe the strength of an eddy it is defined as:

$$\omega = \nabla \times v = \frac{\partial v}{\partial x} - \frac{\partial u}{\partial y} \tag{4}$$

where u and v are the zonal and meridional velocity components, respecitvely. The vorticity describes how the horizontal velocity vector changes in the direction perpendicular to it. The relative vorticity is the vertical component of the rotation, being positive (negative) if the curl turns counter-clockwise (clockwise), compare Figure 3. In the northern hemisphere negative (positive) relative vorticity describes a positive (negative) sea level anomaly (SLA), therefore a clockwise (counter-clockwise) curl and is called anticyclone (cyclone).

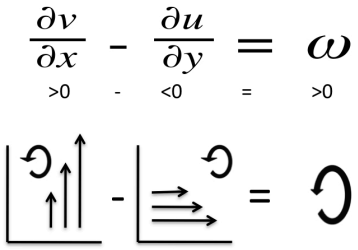

Figure 3: Example for a positive vorticity (cyclonic rotation)

In theory the anticyclones and cyclones must propagate in a westward direction, due to the so-called β-effect. This is independent of the exact shape of the vortex [Van Leeuwen (2006)] The Coriolis force decreases with latitude and vanishes at the equator. In Figure 4 the force balance on the northern hemisphere for an anticyclone is shown. A reasonably large curl has a big enough extent to have different Coriolis parameters at its northern and southern edges. Hence the pressure gradient force, which is equal at both edges, is not balanced

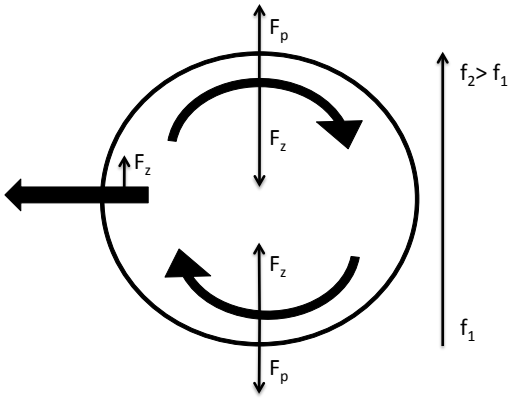

Figure 4: Force balance on an anticyclone in the northern hemisphere.

equally. As a compensation, the β-drift introduces an additional westward velocity, so an additional Coriolis force term, which compensates for the imbalanced force. The β-effect gives a general expectation of the propagation behaviour of eddies in the region of interest.
As mentioned before barotropic or baroclinic instabilities of currents could generate mesoscale variability. To study the region with regard to possible generating places and mechanism of mesoscale variability the currents in the region must be known precisely. This allows a better understanding of possible generating processes and gives an overview over the region.
The region of interest in this study is the tropical northeast Atlantic off northwest Africa (Figure 5b). To understand the circulation and influence factors within that area a bigger overview over the whole tropical and subtropical Atlantic is necessary (Figure 5a). Therefore the subtropical and tropical Atlantic is discussed, before focussing on the smaller region off the northwest coast of Africa.

1.4 Upper circulation of the subtropical and tropical Atlantic

The near surface circulation of the tropical Atlantic Ocean is a result of the interaction between the wind-driven circulation and the global overturning circulation. In the following section the prevailing wind field and the associated meridional overturning of the upper ocean the so-called shallow subtropical cells (STCs) are described. Accordingly the shadow zone is introduced and the zonal equatorial current bands explained.

1.4.1 Wind systems and the Intertropical Convergence Zone

The wind systems and therefore the near surface circulation are dominated by the migration of the intertropical convergence zone (ITCZ). The ITCZ has a general northward displacement in the Atlantic ocean. In boreal summer it is located at the most northern position, around 20°N in the east Atlantic off the African coast and in boreal winter at the most southern around 0°S/N. Within the ITCZ the air is becoming warmer and rises accordingly. In the upper troposphere the air masses flow northward (southward) and sink down in the area of the subtropical high at 30°N (S). This meridional atmospheric circulation is called the Hadley-Circulation.
Due to the meridional pressure gradient from 30°N (S) to the equator and the deflection due to the Coriolis force, the northeast and southeast trades develop and converge at the ITCZ. Directly at the equator, unaffected by the Coriolis force, a zonal pressure gradient from east to west develops and results in a zonal circulation, which is called Walker Circulation. It

describes air rising in the west and sinking in the east. These are the dominant wind patterns, which are the main drivers for the tropical and subtropical shallow ocean circulation; compare the schematic of Figure 5a.

1.4.2 Subtropical Cells (STC):

The STCs are shallow (above 500m) meridional overturning cells that connect the subduction zones of the subtropical gyres of both hemispheres with the eastern, equatorial (during boreal summer) and northern/southern tropical upwelling regions [Schott et al. (2004)].

The north equatorial current (NEC) and south equatorial current (SEC) are the equatorial components of the large-scale anticyclonic subtropical gyre circulations of the northern and southern hemisphere. Within these subduction areas, marked by the blue shading areas in Figure 5a, oxygen rich waters are subducted and ventilate the thermocline. Along the African coast and south of the Cap Verde Islands upwelling is present, which is marked by the green shading.

These two areas are connected through equatorward advection within the thermocline and poleward wind-driven surface flow. The equatorward pathways under the surface layer are represented in Figure 5a by the dotted lines. There are also transport estimates marked for interior and western boundary pathways. Within the subtropical gyre two different water masses are formed, central water by Ekman pumping and subduction into the thermocline and mode water due to mixing and open ocean convection, which is entrained into the thermocline by lateral induction. The water downwells along isopycnals as it moves towards the equator due to Sverdrup dynamics and is transported equatorwards either in the western boundary currents or following interior pathways. The cell is closed by the poleward surface flow, driven by Ekman dynamics.

This process is marked in Figure 5a by the magenta arrows, which represent surface drifter pathways [Grodski and Carton (2002)]. Measurements have shown that subduction rates of both hemispheres are of equal strength [Karstensen and Quadfasel (2002)]. However, most of the subducted water of the northern hemisphere recirculates within the NEC in the Gulf stream and back to the north. In the southern hemisphere the subducted water is transported within the SEC to the northwest. Off the coast of Brazil the SEC splits up into two branches at 12°-15°S. The southern branch recirculates in the subtropical gyre and the northern branch flows into the north Brazil undercurrent (NBUC), which transports most of the southern STC water equatorwards. Around 5°S the NBUC resurfaces and flows northward as a surface intensified current. On its way to the north the north brazil current (NBC) feeds the zonal

current bands of the equatorial undercurrent (EUC) and the north equatorial undercurrent (NEUC), whereas the south equatorial undercurrent (SEUC) is mainly fed from interior recirculations [Böning et al. (2005)]. The current bands will be explained in more detail later in *1.4.4 Equatorial current bands*. However, the eastward undercurrents are the main flow branches, transporting water masses at the Equator to the east underneath the surface layer. The water resurfaces at the upwelling areas of the equator and off northwest and southwest Africa.

The weaker recirculation of the subducted water masses of the southern STC is one reason why the southern STC has a stronger influence on the water mass properties of the upwelling regions, than the northern STC [Ganachaud and Wunsch (2000)].

The NBUC and NBC are the fundamental currents in the Atlantic, which transports surface near water over the equator to the north and therefore are the upper part of the global overturning cell, which is closed due to a transport of cold north Atlantic deep water (NADW) towards the southern hemisphere by the deep western boundary current (DWBC).

Another reason for the different transports of the northern and southern STC is that the interior pathways are more circuitous in the northern hemisphere. Under the ITCZ, surface wind stress curl pumps the pycnocline up toward the surface and vertically compresses density surfaces. This generates a ridge of high potential vorticity, which inhibits the flow of water between the subtropical and equatorial Atlantic [Malanotte-Rizzoli et al. (2000)].

1.4.3 Shadow Zones

According to the theory of the ventilated thermocline [Luyten et al.(1983)] there must be areas at the eastern side of the Atlantic where little ventilation occurs. The upwelling-region southwest of the NEC is not a part of the anticyclonic gyre circulation [Hagen, (2001)] and not directly reached by the equatorial current bands or the interior pathways of the STC. The interior pathways follow surfaces of equal vorticity and the region southwest of the NEC off the African coast comprises a ridge of high vorticity. Therefore the area is weakly ventilated, has nearly no seasonal ventilation and hence is called a shadow zone. Because of the effect of weak ventilation and consumption an OMZ develops. The OMZ is located northeast of the equatorial current system and southeast of the NEC [Stramma et al. (2008)].

1.4.4 Equatorial current bands

The dynamic processes of the upper equatorial Atlantic ocean are mainly wind-driven and consist of a complex pattern of vigorous zonal currents (Figure 5a), which also underlies seasonal fluctuations. One consequence of the mentioned migration of the ITCZ, the northward shift in boreal summer, is the intensification of cross-equatorial southerlies. In boreal winter the ITCZ moves to the equator and the cross-equatorial southerlies weaken. The consequence is a climatic asymmetry (northward displaced ITCZ); the surface winds at the equator are southeast the whole year, strengthening in boreal summer and weakening in boreal winter in response to the seasonal migration of the sun [Okumura and Xie (2004)].

Due to the prevailing wind field from east to west, warm surface waters are pushed to the west of the Atlantic ocean. This leads to a tilt of the thermocline, with a shallower thermocline depth in the central and eastern compared to the western equatorial Atlantic. Driven by this pressure gradient, the equatorial undercurrent (EUC) flows underneath the near-surface layer directly at the equator and transports saline subtropical water to the east. The depth of the core and the transport decreases from west to east and reaches its maximum in late boreal summer and autumn [Brandt et al (2006)], when the cross-equatorial southerlies intensify. On the surface the SEC, splits up into two branches the north SEC (nSEC) and the central SEC (cSEC) and flows westwards at about 2°N and 4°S, respectively. It is strongest in boreal summer with speeds of 55cm/s [Brandt et al (2010), Foltz et al (2003)].

Close to the latitude of the ITCZ (depending on the season 5°N-10°N) the North Equatorial Counter Current (NECC) is located, an eastward current which is strongest during summer and autumn with speeds of 35cm/s [Foltz et al (2003)]. The NECC is fed from the retroflection of the NBC. The NECC feeds into a cyclonic circulation pattern centred at 9°N 25°W in boreal summer and 10.25°N and 22°W in boreal winter, which is called the Guinea Dome (GD). A wind stress curl due to the trade wind system generates the GD. It is a permanent quasi-stationary circulation, described by an uplift of the isotherms in the upper 300m and has a dominating influence on the central water [Stramma (2008)].

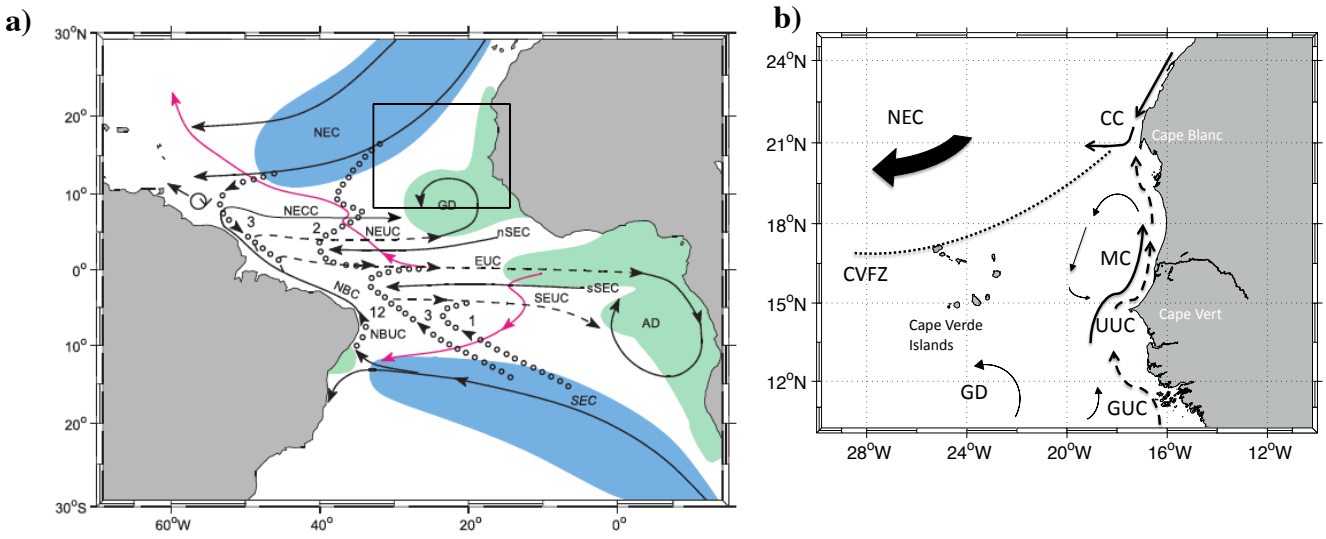

Figure 5: Schematic representation of the Atlantic equatorial circulation branches after *Schott et al. (2004)*.

a) Subduction (blue) and upwelling (green) areas. Current branches are North/South Equatorial Current (S/NEC), South/North South Equatorial Current (n/sSEC), North Equatorial Counter Current (NECC), Equatorial Undercurrent (EUC), North/South Equatorial Undercurrent (N/SEUC), North Basil Current (NBC) and the North Basil Undercurrent (NBUC). GD and AD are the Guinea Dome and Angola Dome, respectively. Interior equatorward thermocline pathways are dotted and transport estimates are added for interior and western boundary pathways. Surface drift is marked due to magenta arrows (from drifter tracks, *after Grodsky and Carton (2002)*.
b) Schematic representation of the circulation in front of the coast of Mauretania. Constructed after *Mittelstead (1991)*, *Pena-Izquierdo et al. (2012)*, the *Disertation of Jens Schafstall (2010)* and the ADCP Measurements of six ship cruises. Canary Current (CC), Upwelling Under Current (UUC), Guinea Upwelling Current (GUC), Mauretania Current (MC) and Cap Verdi Frontal Zone (CVFZ).

1.5 Upper circulation of the tropical northeast Atlantic

The region of the tropical northeast Atlantic is a boundary currents system under the influence of the northeastern trade winds. Therefore wind enhanced coastal upwelling of cold, nutrient rich water and a high biological productivity are attributes of this area. Due to the north/south migration of the ITCZ and being within the trade wind area, the upwelling has a strong seasonal component. From 10°N to 20°N coastal upwelling is present during boreal winter and spring. Meanwhile between 20°N and 25°N upwelling is present the whole year with maximum intensity in summer. North of 25°N coastal upwelling is only observed in summer and autumn.

1.5.1 Current bands

The circulation off the northwestern African coast is represented in Figure 5b.

North of the Cap Verde Islands the NEC represents the southern flank of the subtropical gyre. The NEC is fed by the canary current (CC), which leaves the African coast in a westward direction into the open ocean at about 21°N. The CC is the weak and broad eastern flank of the anticyclonic subtropical gyre circulation in the North Atlantic. It is wind enhanced, directed equatorwards the whole year and transports cold water from higher latitudes to lower.

South of 21°N the almost meridionally shaped coastal area of Mauretania is located. The shelf is very narrow, parallel to the coast and expands ~30km offshore. In this area a cyclonic circulation cell between 21°N – 15°N and 16°W -19° 30'W is present over the whole year, represented in Figure 5b. The northern flank of the cyclonic cell is the westward going CC at 21°N. The southward going east flank of the cell is detectable in the meridional velocities at 18°N in Figure 6 at about 19° 30' W.

At the position where the NEUC meets the African coast some parts are deflected to the north and result in a sluggish northward current near the coast. This current is called Mauretania Current (MC) and represents the eastward flank of the cyclonic circulation cell. The strength of the MC is in strongly connected to the seasonal varying strength of the NEUC. The NEUC has its maximal eastward velocities in August (ITCZ most north) and is very slow and from time to time vanishes completely in boreal spring. For these reasons in winter and spring the MC only reaches latitudes of 14°N, is very weak (Figure 6a) and the prevailing wind pattern result in coastal upwelling between 14°N and 20°N.

During summer and autumn when the NECC strengthens and the northeast trade winds weaken, the MC reaches latitudes up to 20°N and its highest velocities (Figure 6b). During this time no coastal upwelling takes place in that area. The MC transports warm, low saline water from the tropics as far as Cape Blanc [Mittelstaedt (1991)]. North of 20°N strong southwest trade winds prohibit a further northward flow.

The rising of the isopycnals during winter months near the coast in Figure 6a and the lowering during the summer months Figure 6b, shows the seasonal presence of upwelling at the coast, when colder water is upwelled. Due to this rising of the isopycnal a geostrophic poleward undercurrent develops, which is called the upwelling undercurrent (UUC). It is detectable in northward velocities in Figure 6a directly at the topographic slope (16°30'W) at a depth of 50 to 150m. Its mean transport estimations are about 1 Sv and it is the main supply for the coastal upwelling system of south Atlantic central water (SACW) from the south [Dissertation Jens Schafstall (2010)]. The UUC is also fed from the northern branch of the NECC as well as through parts of the NEUC. The UUC seems to be very variable [Mittelsteadt, (1991)], and sometimes connected to northward current velocities of the MC within the surface layer over the continental margin. In contrast to this north of 21°N, where the CC is still at the margin, the UUC deepens, but is still detectable up to 28°N in water properties and velocity [Tomczak (1973), Mittelsteadt (1991)].

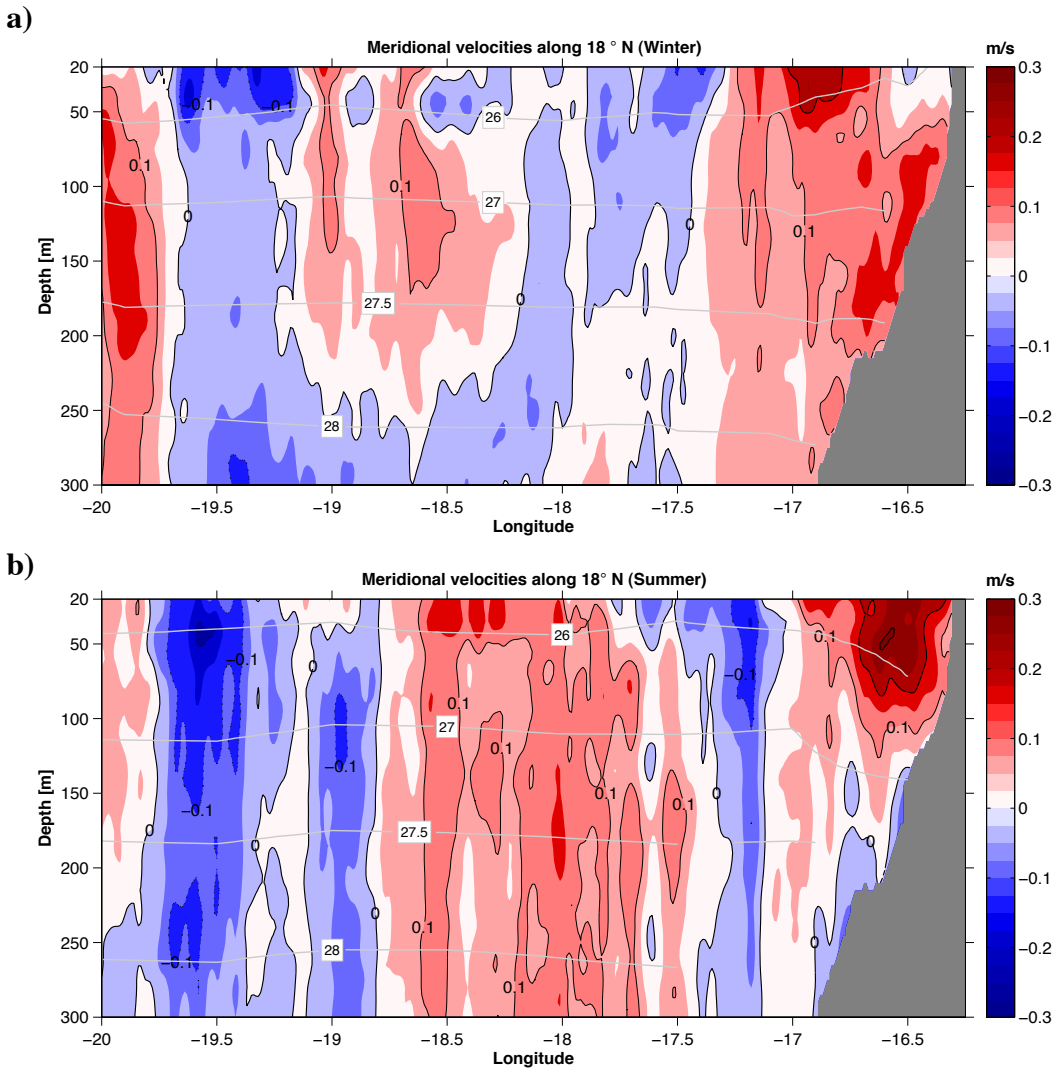

Figure 6: Mean meridional velocity along 18°N from Ship-ADCP measurements of five ship cruises, subdivided into boreal winter (a) (cruises: Poseidon 347, Poseidon 348 and L'Atalante 3) and boreal summer (b) (cruises: Meteor 68/3 and Poseidon 399). White contour lines are density layers out of the CTD stations on the 18°N section.

In conclusion the currents near the coast south of 20°N are northwards directed most of the year. In winter and spring months the wind enhances the equatorward flow directly near the coast, compare Figure 6b, and produces coastal upwelling. This is also detectable from the vertical displacement of the isopycnals in Figure 6. The strength of the upwelling depends on the strength of the winds.

Also during the upwelling season (winter, spring) a poleward flow under the surface almost over the whole shelf is detectable (Figure 6a) and must be seen in connection to the UUC.

As soon as the trade winds weaken the surface flow will be northward again. Therefore a yearly inversion of the flow direction directly at the surface near the coast is detectable, however the subsurface current over the continental margin is poleward all year.

In summer the equatorward current at 19° 30'W and the MC accelerate. The reason for this is not entirely clear. Most likely it is due to strong southeast winds near the equator which generate coastal Kelvin waves. However, deeper at 175m-250m at the shelf no northward velocities are present any more, this must be due to the weaker UUC which is missing due to the fact that there is no upwelling.

Model runs show that the coastal upwelling is mainly fed from the southern hemisphere [Glessmer et al. (2009)]. This would be consistent with the idea of the pathway from the southern STC, which transports water from the south via the NBC and the NEUC to the east. This connection could be conjectured from observed water mass properties and some zonal and meridional velocity sections. An attempt to demonstrate the connection with 12 Argo floats, released in the western tropical Atlantic at 200m depths, adduced the result that no one reached the region east of the Cap Verde Islands [Stramma et al. (2008)]. Maybe floats should be isopycnal to establish this connection.

1.6 Water masses of the upper tropical Atlantic

A T/S diagram has been created to gain a better overview over the water mass properties and their origin (Figure 7). Argo-Profiler provide information about the T/S properties of the water masses in the upper 2000m (27.7kg m^{-3}) of the water column, which is the water column of interest in this study.

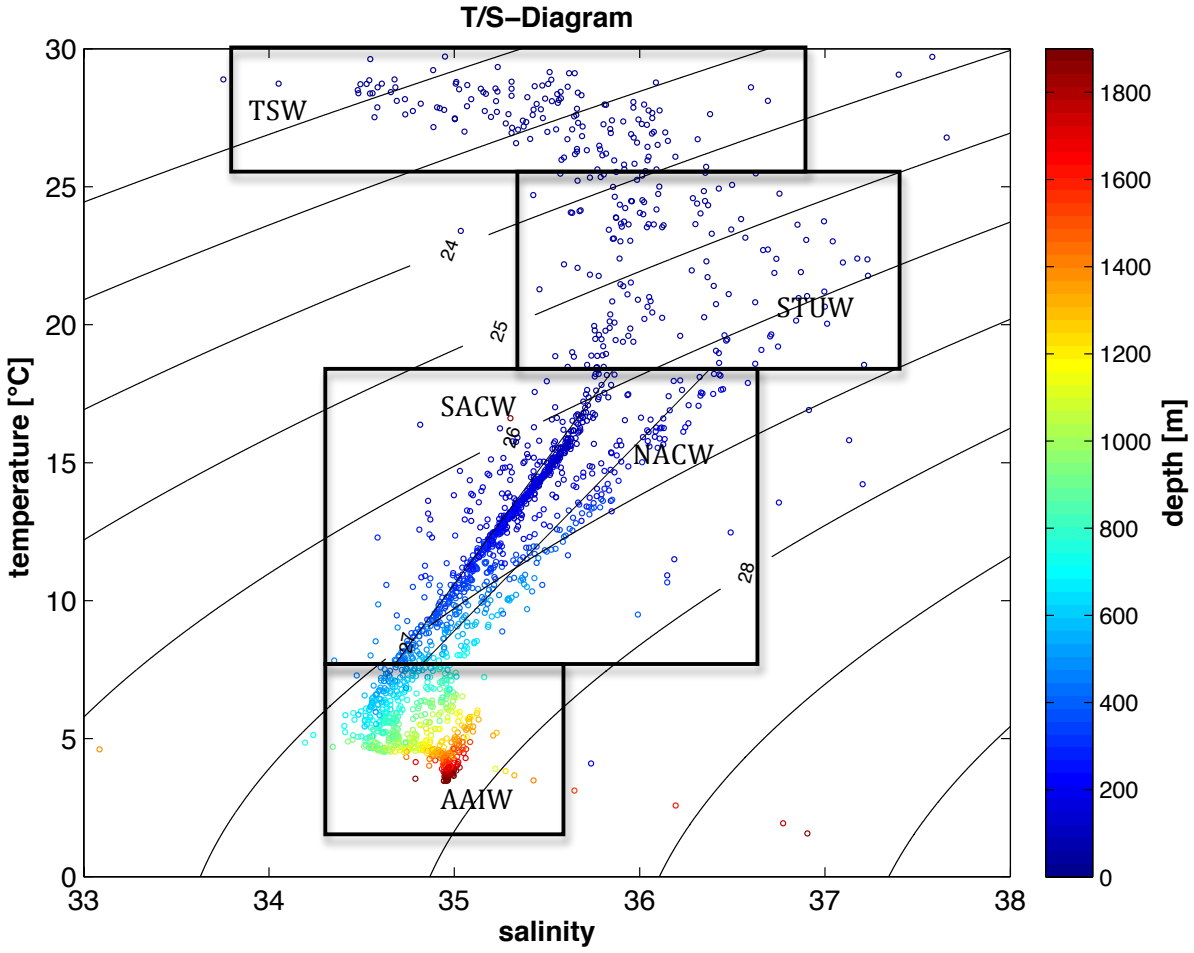

Figure 7: Temperature / Salinity diagram constructed from Argo-Profiles carried out in the tropical northeast Atlantic (0° - 20°N, 10°W – 30°W) over the last eight years. Boxes describe the tropical surface waters (TSW), the subtropical underwater (STUW), the north Atlantic and south Atlantic central waters (SACW and NACW) and the Antarctic intermediate water (AAIW). The contour lines are the potential density surfaces.

The warm very light water (σ_θ < 24.8 kg m^{-3}) is the tropical surface water (TSW), which is in direct contact with the atmosphere. In the tropics a typical mixed layer thickness is 10 to 100m. Due to the direct contact to the atmosphere the TSW has high oxygen concentrations. Directly beneath the surface layer the subtropical underwater (STUW) is located. It is characterized with by a maximum in salinity and has its origin in the central subtropical gyre. The almost linear relationship from warm and saline towards colder and fresher water masses, between the density layers σ_θ = 25.8 kg m^{-3} and σ_θ = 27.1 kg m^{-3} is characteristic for the

central waters (CW). The CW can be divided into two different water masses of the southern and northern hemisphere, the north Atlantic central water (NACW) and the south Atlantic central water (SACW). The NACW originally develops in the north Atlantic subduction zone. The Cap Verde Frontal Zone (CVFZ) separates these two central water masses. South of the CVFZ, the SACW dominates which has its origin in the southern hemisphere subtropical gyre subduction zone. SACW has a lower salinity and is colder than the NACW. Furthermore the SACW is low in oxygen, nutrient-rich and reaches depths of about 600m in the tropical Atlantic. Both water masses can be seen in the T/S diagram as two parallel linear temperature/salinity relationships. The Antarctic intermediate water (AAIW) is located beneath the CW in depths between 600m and 900m and has densities between $\sigma_\Theta = 27.1$ kg m^{-3} to $\sigma_\Theta = 32.15$ kg m^{-3} in the tropical Atlantic. The AAIW has its origin in the subpolar regions around Antarctica, is produced by subduction and spreads from the southern ocean into all ocean basins. It is characterized by its minimal salinity.

2. Data

In this chapter the data, which is used for this work, is introduced. In the first section the satellite data and the Argo data are described. After that the research cruises and mooring work, which was carried out in the last seven years by GEOMAR in the area of the tropical northeast Atlantic is detailed.

2.1 Satellite data

Satellites provide useful datasets for studying the world oceans over the last decades. They supply information about different oceanographic parameters from the ocean surface with good coverage and continuity. Satellite derived parameters that are used in the work and described briefly in the following are SLA, Sea Surface Temperature (SST), Chlorophyll (Chl) and sea surface wind stress.

2.1.1 Altimeter derived Sea Level Anomaly

To examine the ocean mesoscale dynamics, the satellite dataset of the SLA is extensively used, because for the first time temporal and spatial scales of eddies are clearly represented, as well as eddy behaviour and pathways. The Topex-Poseidon satellite mission was shut down after 14 years in 2006. Henceforth three satellite missions (Jason 1, Jason 2 and Envisat) are operating in the orbit at the same time providing precise measurements. Figure 8 shows the shifted cycles of the three different satellite missions for a better coverage. The three different data packages will be merged together to one dataset, which will be briefly explained later. All of the altimeter missions sample regularly every second, which is equivalent to every 7 km along their ground track [Morrow and Le Traon (2007)]. Jason 1 and Jason 2 have an orbit which is not sun-synchronous and repeat their track in less than10 days, whereas Envisat is in a lower sun-synchronous orbit and needs exactly 35 days for one cycle [AVISO]. Unfortunately the contact to Envisat shut down on 8th of April 2012 and the Envisat mission

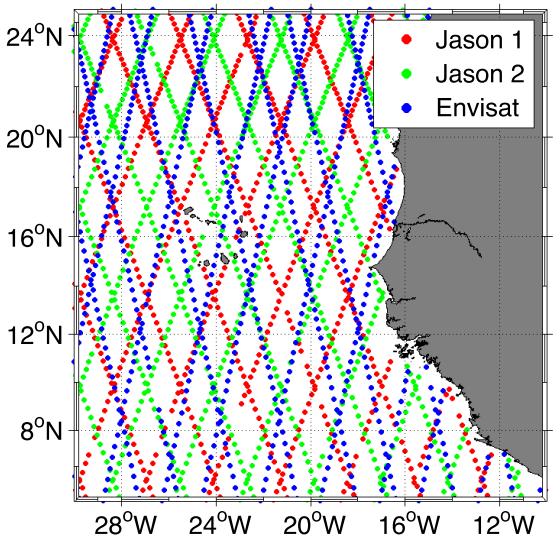

Figure 8: Coverage of the altimeter missions in the tropical northeast Atlantic between the years 2000 and 2011. Jason 1 (red), Jason 2 (green), Envisat (blue).

will not be continued. Nevertheless, for the period of time, which is examined in this work (2000-2011), the Envisat mission was in operation.

The dataset of the SLA delayed time references, which are used in the study, is provided by AVISO (Archiving, Validation, and Interpretation of Satellite Oceanographic) [http://www.aviso.oceanobs.com/]. SLA stands for the difference between sea surface and the mean sea level topography. The data consists of all the different satellite missions to get a good coverage. Difficulties are, that the ground track pattern from the different missions do not have the same space-time coverage (Fig. 8), furthermore each mission has different error budgets and orbit differences, which leads to large scale biases and trends [Morrow and Le Traon (2007)]. All these errors need to be corrected as well as possible. In consideration of these problems the SSALTO/DUACS project constructs data sets onto a 1/3° x 1/3° Mercator grid every 7-10 days. For more information about the merging interpolation technique, see [Morrow and Le Traon (2007)] or the AVISO User Handbook.

The chosen dataset ranges from 01.01.2000 to 31.12.2010 and has a time resolution of one day. As completely independent data exists only at a minimum of seven days, this one day resolution is an average of the seven days. The study area reaches from 10°N – 25°N and 13°W to 28°W. To detect submesoscale features it must be kept in mind that a 1/3° grid really resolves only Gaussian shaped eddies with a radius >50km [Alpers et al. (2013)]. Smaller eddies could also be detected but the energy below ~50km is damped due to the 1/3° grid and the merging.

2.1.2 Sea Surface Temperature

The data from the SST, which are used in this study are from the radiometer on board the NASA satellites, within the Tropical Rainfall Measuring Mission (TRMM). The data is available from the SSMI Homepage [www.ssmi.com]. For the surface temperature records the TMI (TRMM Microwave Imager) radiometer is used. The TMI is a 9-channel, passive radiometer that operates in the frequency range between 10.65 and 85.5 GHz. The channel that operates in the lowest frequency is able to collect data through cloud cover [Athie and Marin (2008); Grodsky et al. (2005)], this is a great advantage especial in areas like the tropics where cloud coverage is expected. Because of this there are rarely to data gaps caused by faulty samples and a nearly complete daily coverage of the area between 40°S and 40°N is achieved. The data set used in this study reaches from 10°N – 25°N and 13°W to 28°W, on a ¼ ° x ¼ ° grid. It is available on a daily basis, but as a running three-day mean value.

2.1.3 Chlorophyll

A moderate resolution imaging spectoradiometer (MODIS) is aboard the Terra and Aqua satellites, their orbits are shifted, so that they are together able to monitor the complete earths surface every 1 or 2 days. MODIS is able to acquire data in 36 spectral bands.

The chlorophyll data is available at www.oceancolor.gsfc.nasa.gov and is downloaded for the region between 10°N – 25°N and 13°W to 28°W for the year 2011.

2.1.4 Sea surface windstress

The scatterometer climatology of ocean winds (SCOW), which is provided by Risien, C.M. and D.B. Chelton, which computed the wind fields using the method explained in Risien C.M. and D.B. Chelton (2008), is available at http://cioss.coas.oregonstate.edu/scow/ineex.html. It is used to get an overview over the seasonality of the wind stress in the region of the tropical northeast Atlantic. The climatology is based on 122 months from September 1999 until October 2009 and is available on a global 2°x2° grid. The data is produced from the QuickSat satellite, which is on a sun-synchronous orbit (830km) with a microwave radar (f=13.4 GHz) onboard, that measure near-surface wind speed and direction under all weather and cloud conditions [NASA-SeaWinds on QuickSCAT]. The radar covers a 1.800km wide band and makes approximately 400 000 measurements a day. The satellite covers 90% of the earth surface within one day.

2.2 Argo Profiler

Autonomous conductivity temperature device (CTD) profiling floats of the Argo program were used to investigate the vertical structure of the area. The Argo-Program consists of a big collection of drifting buoys that are deployed worldwide. The buoys measure temperature, conductivity, pressure and can dive up to 2000m. At the ocean surface, after completing a profile, they send their data via satellite to a data collecting centre and the data is freely available at http://www.coriolis.eu.org. The data set used in this study reaches from 01.01.2004 to 31.12.2011, during this time 10.446 profiles were carried out in this area.

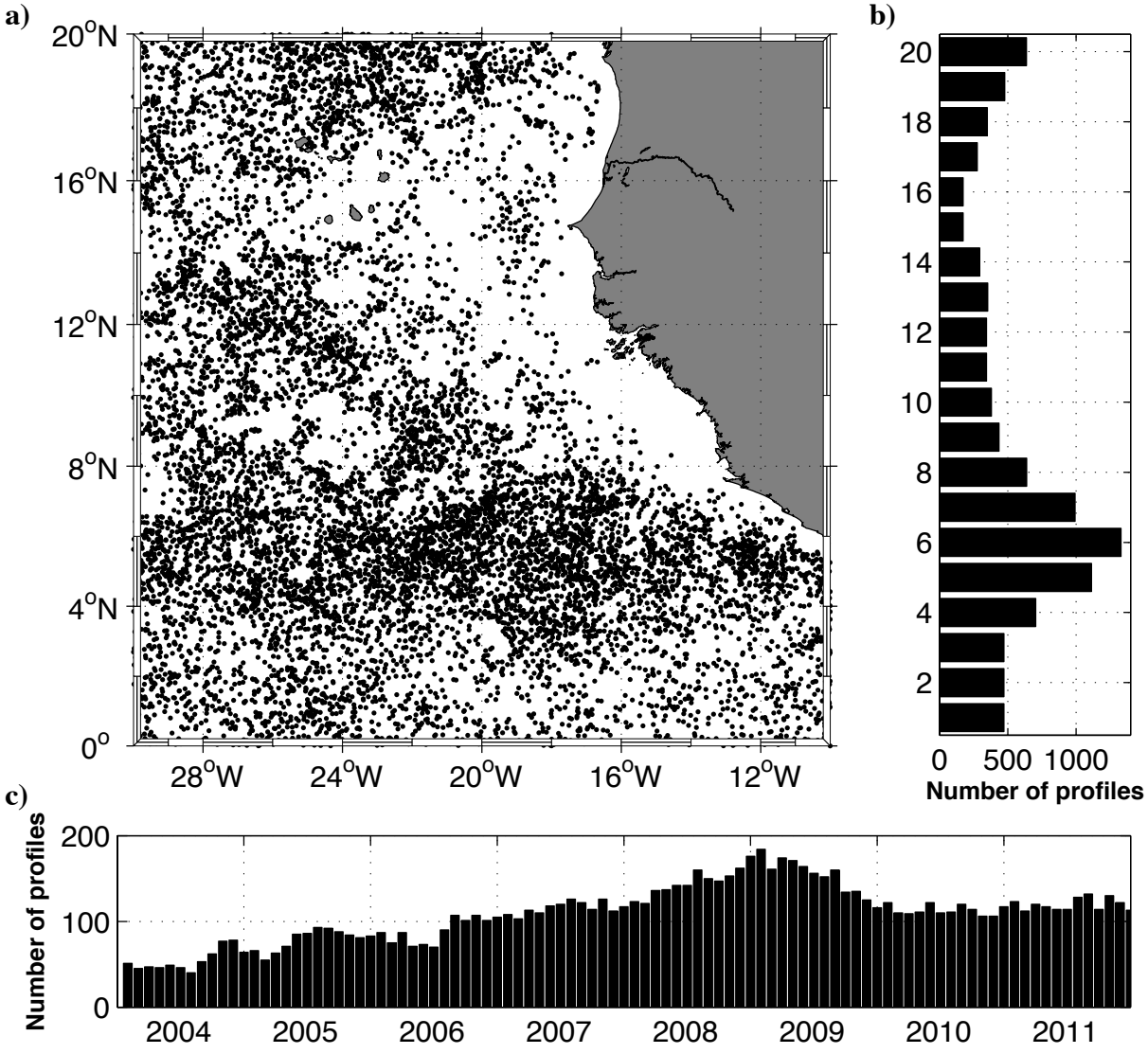

Figure 9:
a) Spatial distribution of the 10446 profiles, done between 01.01.2004 and 21.12.2011.
b) Meridional variation of the number of Argo profiles, done in the same time span.
c) Monthly variation of the number of profiling floats between 2004 and 2011.

Figure 9 shows some statistics about the number of profiles done between 2004 and 2012 years in the tropical northeast Atlantic. In Figure 9a) the spatial distribution of all 10.446 profiles carried out between 0° - 20°N and 10°W – 30°W are shown.

The shadow zone of the North Atlantic is hardly reached by the drifting Argo profiler and clearly visible in the map around 10°-18°N and 16°W-24°W. In the 1° latitude bands of the meridional variation of the number of Argo profiles (Figure 9b) a very low number of profiles between 13°N and 18°N represent this fact as well. The most profiles carried out between 4-8°N which is in the area of the zonal eastward NECC. The monthly variation of the number of Argo profiles (Figure 9c) shows that we had a constant increase of Argo profiling floats until the year 2008. In the following year there was a decrease, but since 2010 there is a constant number of ~100 profiles from Argo floats a month.

2.3 Ship cruises

Oceanographic data was collected in 6 ship expeditions into the upwelling region off the coast of northwest Africa. Most of them started at the Cap Verde Islands and were carried out along 18°N into the upwelling region off the coast of Mauretania (Figure 10). Four of these cruises were carried out between boreal winter/spring during strong upwelling phases and two cruises in the summer months, when no strong upwelling is present, compare Table 1 for details.

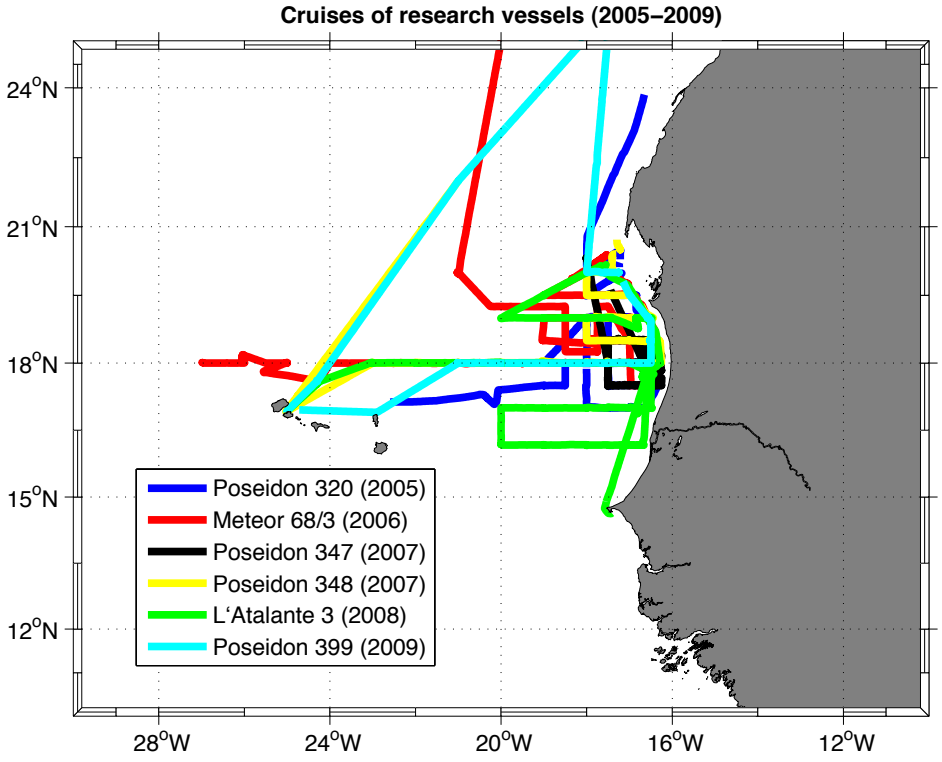

Figure 10: Map of all cruises into the northeast Atlantic.

Expedition	Time	Cruise Report
Poseidon 320	March-April 2005	Bange (2008a)
Meteor 68/3	July-August 2006	Körtzinger (2009)
Poseidon 347	January-February 2007	Dengler et al. (2008)
Poseidon 348	February 2007	Bange (2008b)
L'Atalante 3	February 2008	Körtzinger (2008)
Poseidon 399	May-July 2009	Dengler et al. (2009)

Table 1: Expeditions with the appropriate cruise report.

2.3.1 Vessel mounted Acoustic Doppler Current Profiler

During the six expeditions the velocities in the upper layers of the water column were measured ongoing with an Acoustic Doppler Current Profiler (ADCP), which is fixed embedded into the research vessels. An ADCP uses the Doppler effect to measure current velocities in the water column. It sends out acoustic waves and receives the reflection from particles or any disturbance of the sound velocity within the water column. Under the assumption the particle moves within the ocean current one can conclude from the measured Doppler shift on the velocity of the current. The ADCP on board the Poseidon and the Meteor is called a 75 kHz Ocean Surveyor and is build by RD Instruments. 75 kHz is the frequency the ADCP is working with and responsible for the length of possible backscatter, in this case $\lambda = c/f \approx 2$ cm.

On board the R/V Poseidon and the R/V Meteor most of the time, the ADCP was used with a vertical resolution of 8m whereby the range is >500 m. Inside the French research vessel, L'Atalante, two ADCPs were used in the following resolution, a 300 kHz ADCP with a vertical resolution of 4 m and a range of <150 m and a 75kHz ADCP with a vertical resolution of 16m and a range of 400 m.

For data recording the data acquisition system (DAS), which is provided by RD Instruments, was used and the data processing was done with standard techniques for calibration [Fischer et al. (2003)]. A possible difficulty is that an exact knowledge of the installation angle inside the ship is necessary to ensure that false measurements do not occur due to the movement of the ship.

The accuracies for one hour ensembles, taking an underway measurement in the tropics during calm sea, from the different ADCP's are represented in Table 2 [Fischer et al. (2003)].

Research Vessel	ADCP	Frequency	Bin length	Ping rate	Accuracy
R/V Poseidon	Ocean Surveyor	75 kHz	8 m	2,5 s	~5 cm s^{-1}
R/V Meteor	Ocean Surveyor	75 kHz	8 m	2,4 s	~5 cm s^{-1}
R/V Meteor	Ocean Surveyor	38 kHz	16 m	2,8 s	~5 cm s^{-1}
R/V L'Atalante	Narrow band ADCP	75 kHz	16 m	2,4 s	~5 cm s^{-1}
R/V L'Atalante	Narrow band ADCP	300 kHz	4 m	1,0 s	~3 cm s^{-1}

Table 2: Measuring inaccuracy for 1-h- ensembles from the used vessel mounted ADCPs. [Personal communication with Jürgen Fischer and Rainer Zantopp]

2.3.2 Conductivity temperature depth

To measure vertical structures of oceanographic properties like salinity, temperature, pressure and among other things oxygen, a CTD-rosette is lowered from the research vessel on all cruises at specific stations. The vertical distribution of properties is measured on all cruises by a Seabird Electronics Device (SBE 911 plus). Niskin bottles are installed to make in situ calibration of the conductivity and oxygen sensor and to measure other chemical or biological properties. Salinity is specified due to the conductivity measurements, which are calibrated with the Autosalinometer measurements of water samples. The calibration for the oxygen sensor is carried out, comparing the measurements to values determined by a titration using the Winkler method. The in situ calibration led to the following accuracies:

Research cruise	No. of Profiles	Salinity	Oxygen
Poseidon 320	42	0.005	1.74 µmol/kg
Meteor 68/3	96	0.002	2.61 µmol/kg
Poseidon 347	126	0.005	3.05 µmol/kg
Poseidon 348	33	0.005	3.05 µmol/kg
L'Atalante 3	61	0.003	3.05 µmol/kg

Table 3: Inaccuracies of the salinity and oxygen measurements

2.4 Cap Verde Ocean Observatory Mooring

The Cap Verde Ocean Observatory (CVOO) is a deep-sea moored instrument array deployed at a depth of about 3600m, 60km northeast of the Cap Verde Islands. The exact mooring position at the moment is 17° 35.39'N, 24°15,12'W. The mooring was first deployed on 08.06.2006 and has been redeployed five times keeping it in constant use until today. The

dates of redeployment are March 2008, October 2009, May 2011 and October 2012.

An ADCP was installed during all periods at ~100m depth directed to the surface, measuring water velocities to the surface.

The temperature und salinity measurements from the upper 350m used in this work are carried out from 8 Microcats positioned at depth of ~30m, ~50m, ~70m, ~100m, ~120m, ~200m, ~300m and ~400m along the mooring. In 2007 all instruments were 12m higher in the water column and 2010 10m lower.

The oxygen measurements used in this work are carried out by an optode, which was installed at about 100m in 2007 and at about 45m in 2010. The optode was calibrated before and after the mooring deployment.

3. Methods

The first idea was to study the mesoscale variability within the region of interest by counting, with the help of the SLA, Argo floats which were making their profile within an anticyclone, a cyclone or outside of an eddy. Interpretation of the different profiles enabled, for example, Chaigneau et al. (2011) to study the vertical structure of eddies in the eastern Pacific. But in the region of the tropical northeast Atlantic the small number of Argo profilers (see Figure 9a) does not enable significant results.

The goal of this work is a general statement about the eddy activity and the description of single eddy events. Therefore it was decided to base the study of the general eddy activity on the data set with the best temporal and spatial distribution, that is the satellite data, and to analyse single eddy events using the datasets which are carried out by the ship cruises and the mooring.

3.1 Argo data

Despite the small number of Argo profiles within identified eddy areas, the dataset (2004-2012) in the tropical northeast Atlantic (0°-20°N; 10°W–30°W) contains in total 10.446 profiles and gives an overview over the water mass properties of the upper 2000m. To build the T/S diagram (Figure 7) only every eighth value from every 10.466 profiles is used. The chosen values are randomly distributed over depth. This is done to downsize the enormous amount of data. The T/S diagram also gives information about the depths of the measurement, accordingly the water mass (colour). Superimposed are the potential density layers.

3.2 Ship ADCP and CTD Stations

The ADCP data of the six ship cruises from 2005-2009 are used to get an overview over the circulation in the area of the tropical northeast Atlantic and to study the vertical structure of single eddy events.

Five cruises, except from the first cruise Poseidon 320 in 2005, carried out an ADCP section with CTD stations every 0.5° along 18°N. These sections are used to created a mean circulation pattern from the upper 300m along 18°N between 20°W and 16.5°W, which is almost perpendicular to the coastline of Mauretania over the shelf into the deep ocean. The different ADCP datasets of each cruise were interpolated on a common grid and than averaged. The resulting circulation pattern is subdivided into a summer circulation pattern

(R/V Meteor 68/3 and R/V Poseidon 399) (Figure 6a) and a winter circulation pattern (R/V Poseidon 347, R/V Poseidon 348 and R/V L'Atalante 3) (Figure 6b). No filter was applied.
In addition the ADCP data were used to explore the dynamics of different eddy-like structures. The ADCP records of all six cruises were visually studied to discover mesoscale eddy features and 15 eddies were identified. An anticyclone and cyclone were chosen to be analysed in more detail. The vertical structure of the velocity is shown in Figure 12. Again no filter was applied.
At the Meteor 68/3 cruise 2006 an anticyclone was located on the 18°N CTD section and five CTD stations were carried out within the eddy (CTD cast: 30, 31, 32, 33 and 34 at 17°W, 17.5°W, 18°W, 18.5°W, 19°W and 19.5°W on 18°N, respectively). So a vertical structure in temperature and salinity could be plotted (Figure 17) as well as the ADCP measurements (Figure 16a). Temperature, salinity and oxygen measured from the CTD are horizontal interpolated on a 0.05° grid. Due to the fact the ship cruises through the eddy were linear, a distance from the eddy centre, which is defined as that point of zero velocity out of the velocity plot, is computed and used instead a longitude value. The data from the SADCP is averaged within every 1/50° longitude, to average out the high amount of measurements during a CTD station.
The Poseidon cruise 348 cut through one further eddy in February 2007, which was selected and plotted (Figure 16b). Unfortunately there were no CTD stations carried out during the eddy crossing.

3.3 CVOO Mooring Data

Also the mooring ADCP dataset from 2006 to 2011 was visually inspected to identify mesoscale eddy structures. Two events both in February 2007 and 2010 attract attention. The ADCP, salinity and temperature measurements were filtered with a 24-hour high pass filter to remove the tides and other short period fluctuations. The distance x-axis is computed with the help of the tracked translation velocity of the eddy, computed from the Eddy-Tracking-Algorithm and the time the eddy needed to cross the mooring position. The centre of the eddy is again selected visually out of the velocity structure.
To get a better understanding of the change of the eddy properties during its lifetime a vertical mixing profile is computed. This is done selecting temperature and salinity in the eddy centre at an early state of the eddy, after eight months at a later development state of the eddy and from the surrounding water. This is done along every 0.05 kg/m^3 density between the 25.6 kg/m^3 and 26.65 kg/m^3 isopycnals. The densities are selected to start beneath the mixed layer.

Assuming that diapycnal mixing does not occur, the lateral mixing ratios along isopycnals could be computed with the help of:

$$\text{Eddy Core Water}_{\text{Later state}}(x_1 + x_2) = \text{Eddy Core Water}_{\text{Early state}} \cdot x_1 + \text{Surrounding Water} \cdot x_2$$

$$\rightarrow \quad x_2 = \frac{\left(\text{Eddy Core Water}_{\text{Later state}} - \text{Eddy Core Water}_{\text{Early state}}\right)}{\left(\text{Surrounding Water} - \text{Eddy Core Water}_{\text{Early state}}\right)} \qquad \textbf{(5)}$$

3.4 Sea Surface Temperature

The SST data is used to show a snapshot of 20.05.2011 between 15°N – 22°N and 15°W to 20°W to show the upwelling and mesoscale variability in the region of interest (Figure 1), for that interest the data is unprocessed and just shown.

In addition, a climatology is built out of the years 2000 to 2010 and is shown as colours underlying the climatology of the surface velocities. In Figure 27 the months February, June, August and December are chosen as representative for their season and plotted.

3.5 Chlorophyll

The unprocessed chlorophyll data is shown as a snapshot of 20.05.2011 between 15°N – 22°N and 15°W to 20°W to demonstrate the nutrient-rich water, the high productivity and the mesoscale variability (Figure 1).

3.6 Windstress

The climatology of the wind stress is plotted from the point 15°09'N and 17°22'30W, which is slightly north of Cap Vert. The data is also unprocessed and is plotted onto the climatology of newly detected cyclones and anticyclones in Figure 27.

3.7 Eddy-Tracking-Algorithm based on SLA data

For detecting eddy-like structure from the SLA data an algorithm based on the Okubo-Weiß-Method is used, which is defined in the works of Okubo (1970) and Weiß (1991). The method is quite robust and widely used, on satellite data as well as on numerical model data [e.g. Isern-Fontanet et al. (2006) and Sangrá (2009)]. The goal is to detect eddies with SLA data, to track them over time, to identify pathways and spatial distributions.

The idea behind the Okubo-Weiß-Method is to determine regions where the relative vorticity, which describes the local spinning motion of a fluid relative to the Earth (see *1.3 Physical*

background), dominates the strain tensors, which contains the stress, which acts on the water parcel. Compare Figure 11a) and c) for the relationship of relative vorticity and the direction of the rotation of the eddy.

The strain tensors describe the stress, which acts on a water parcel and they are classified as 'normal strain' and 'shear strain'. The normal strain is a deformation acting perpendicular to the surface of an element whereas the shear strain is a deformation, which is obtained from forces acting tangential to the surface of an element. The shear (s_s) and normal (s_n) strain can be computed as:

$$s_s = \frac{\partial v}{\partial x} + \frac{\partial u}{\partial y} \qquad s_n = \frac{\partial u}{\partial x} - \frac{\partial v}{\partial y} \qquad \textbf{(6)}$$

In order to obtain surface velocities, which are needed for the calculation of relative vorticity as well as of the strain tensors, the geostrophic approximation was considered to be valid.

So from SLA data the geostrophic surface velocities, u and v, are calculated (Eq.2):

$$fu = -g \cdot \frac{\partial \eta}{\partial y} \qquad fv = g \cdot \frac{\partial \eta}{\partial y} \qquad \textbf{(7)}$$

, where f is the Coriolis parameter, g the acceleration due to gravity and η the SLA. The Okubo-Weiß Parameter (W) evaluates the relative vorticity against the strain tensors:

$$W = s_n^2 + s_s^2 - \omega^2 \qquad [1/s^2] \qquad \textbf{(8)}$$

Areas where W has high negative values gives us regions where the relative vorticity dominates over the strain, this area would be defined as an eddy and the highest value as its centre (Figure 11).

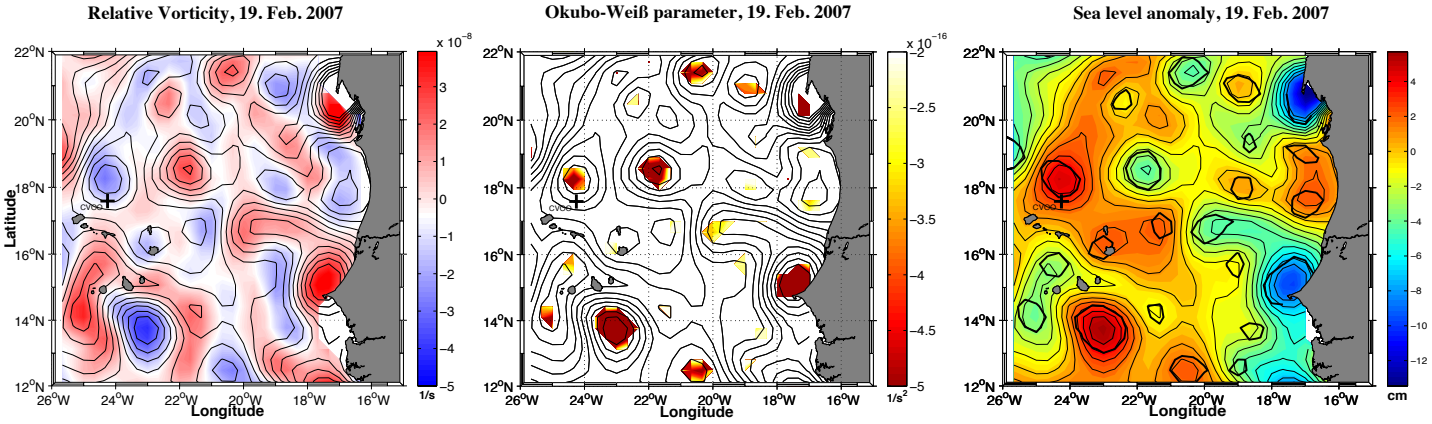

Figure 11: Distribution from 19.02.2007 of **a)** relative vorticity (colour) **b)** Okubo-Weiß-Parameter (colour) and **c)** SLA (colour and thin black lines). Superimposed in **a)** and **b)** are contours of SLA (thin black lines) and in **c)** eddy areas identified by the Okubo-Weiß-Method (closed thick black lines). The black cross marks the mooring position CVOO.

To detect these regions of dominant relative vorticity a threshold value (W_0) is used, so eddies are defined as regions with $W<(-W_0)$ (Figure 11b), called elliptic regions [Souza et al. (2011)]. The eddy core is defined as a region of negative W (vorticity dominates over strain) surrounded by a region of positive W (strain dominates over vorticity) [Souza et al. (2011)]. The results are the encircled regions of $W<(-W_0)$, superimposed on the SLA which gives us the region of an eddy (Figure 11c).

Other conditions of W are $W>W_0$, which is called a hyperbolic region and $|W|<W_0$ which is the background field [Souza et al. (2011)]. The background field has very small magnitudes of W compared to the eddy centres. The original threshold is defined as $W_0=-0.2\cdot\sigma$, with σ being the spatial standard derivation of W [e.g. Isern-Fontanet et al. 2006], but using $W_0=-2x10^{-12}\,s^{-2}$ gives very similar results, so this was used as threshold value instead, which is also done in previous studies e.g. Chelton et al. 2007.

To better identify coherent structures in the resulting field of W some previous studies applied a low pass spatial filter, but this is not done here.

An eddy trajectory was defined only if for the time t an eddy with the same polarity, like the one for the time (t-1) was found within the defined search radius of 10km. Eddies were only tracked if they had a radius of >30km and were visible more than 7 days.

3.8 Analyses of the results from the Eddie-Tracking-Algorithm

The Eddie-Tracking-Algorithm was carried out to capture all eddies generated in or passing the area, to characterise the general eddy activity within the region of the tropical northeast Atlantic, their generating mechanism, distribution, properties and pathways.

To test the robustness of the Eddie-Tracking-Algorithm the results from the selected eddies, from the ship crossing ADCP measurements and the moored ADCP measurements, are compared. Besides the trajectories from the two eddies crossing the mooring position in 2007 and 2010 are plotted (Figure 14) to identify the location of their origin and compare their properties.

To get a better impression on the general eddy activity and the properties of the eddies the Eddie-Tracking-Algorithm is programmed to save the latitude and longitude of the eddy centre, the SLA amplitude [cm], the area of high W which is defined as eddy [km^2], the radius [km], the intensity [(cm^2/s^2)/km^2], the mean EKE [cm^2/s^2] and the mean vorticity [1/s] for every eddy each day. Mean values are shown in Table 4. A long tracked anticyclone and cyclone as well as one anticyclone, which passed the mooring are selected exemplary and

their properties are shown against the time they were tracked (Figure 15 and 19).
To get an indication on possible generation locations of eddies, on a 1°x1° all start positions of trajectories were counted. Every grid box represents the number of trajectories, which start within the box. The result is a spatial distribution of the starting points of trajectories therefore an indication of the possible production places of eddies (Figure 21).
To detect the interannual variability of the general eddy activity in the region, the actual number of newly detected eddies in a year is compared. This is done for all eddies as well as subdivided into anticyclones and cyclones (Figure 22a). To get information about the generation of the mesoscale variability, a count was made of how many newly detected eddies were found eastward of 18°W at the coast over all years (Figure 22b). Also the seasonal variability of the number of detected eddies within one year is shown in Figure 23, as well for all eddies as subdivided into anticyclones and cyclones. A count was made of how many newly detected eddies were found in every month over the time span from 2000 to 2011.

To identify possible pathways of eddies every eddy passing a box is counted in 1/3° x 1/3° boxes, finally yielding a dataset with the unit eddy / box. Only eddies were counted, which were detectable for longer than 90 days and every eddy could only be counted once per box. Then the dataset is interpolated on a high-resolution grid (1/20°) with the Obana interpolation method, to smooth the pathways (x-y influence radius 0.5°, x-y cut of radius 0.8°). To get the direction of the eddies and not just the eddy distribution, some chosen trajectories are superimposed, corridors are framed and arrows show the direction (Figure 24).

3.9 Geostrophic velocities

As mentioned in the chapter *3.7 SLA Eddy Tracking Algorithm* geostrophic surface velocities are computed out of the SLA data in the region between 10°N – 25°N and 13°W to 28°W. In this work they are used to get an overview of the instabilities of the surface boundary current. A climatology from 2000 to 2010 is produced and February, June, August and December are plotted in Figure 27. In addition, as an exemplary year, the year 2000 is plotted in 12 plots showing the monthly mean velocity fields (Figure 28).

4. Results

The results are subdivided into the *4.1 Observations of single eddy events* and the *4.2 General eddy activity, its origin and distribution*. In 4.1 the vertical structure, the kinematic properties and the changes during the lifetime of an eddy are examined, whereas in 4.2 the single eddy event is set into a bigger context with regard to general dynamics. A study is made of the general eddy activity and characteristics within the region, the location of the origin of mesoscale variability and indications of possible generating mechanisms.

4.1 Observations of single eddy events

The eddy structure in in-situ observations is often disturbed by other background flow and is not as clear as in theory. However, to describe the horizontal and vertical structure with oceanographic properties, like velocity, sea level elevation, temperature, salinity and oxygen, chosen measurements of single eddy events are presented as examples.

4.1.1 Vertical velocity structure and SLA signature of a cyclone and an anticyclone

During its cruise A3 on 08.02.08 the R/V l'Atalante crossed an anticyclonic eddy and measured with the SADCP the vertical velocity structure (Figure 12a and c). The satellite data showed on this date and at this location a positive SLA (red shading in Figure 12a) and the black circle around the positive SLA are structures of high |W|, meaning the Eddy-Tracking-Algorithm was able to identify this eddy, too. This is a good test for the robustness of the algorithm, to compare its results to other independent measurements, like the ones collected on ship cruises.

On Figure 12a the cruise track from the R/V l'Atalante is superimposed on the SLA field and presented as the dashed lines. The arrows represent the water velocity, which is measured with the SADC during the cross section over the eddy. Black arrows are the velocity in 61m depth and white arrows in 205m depth. From the arrows the rotation of the anticyclonic eddy, is seen.

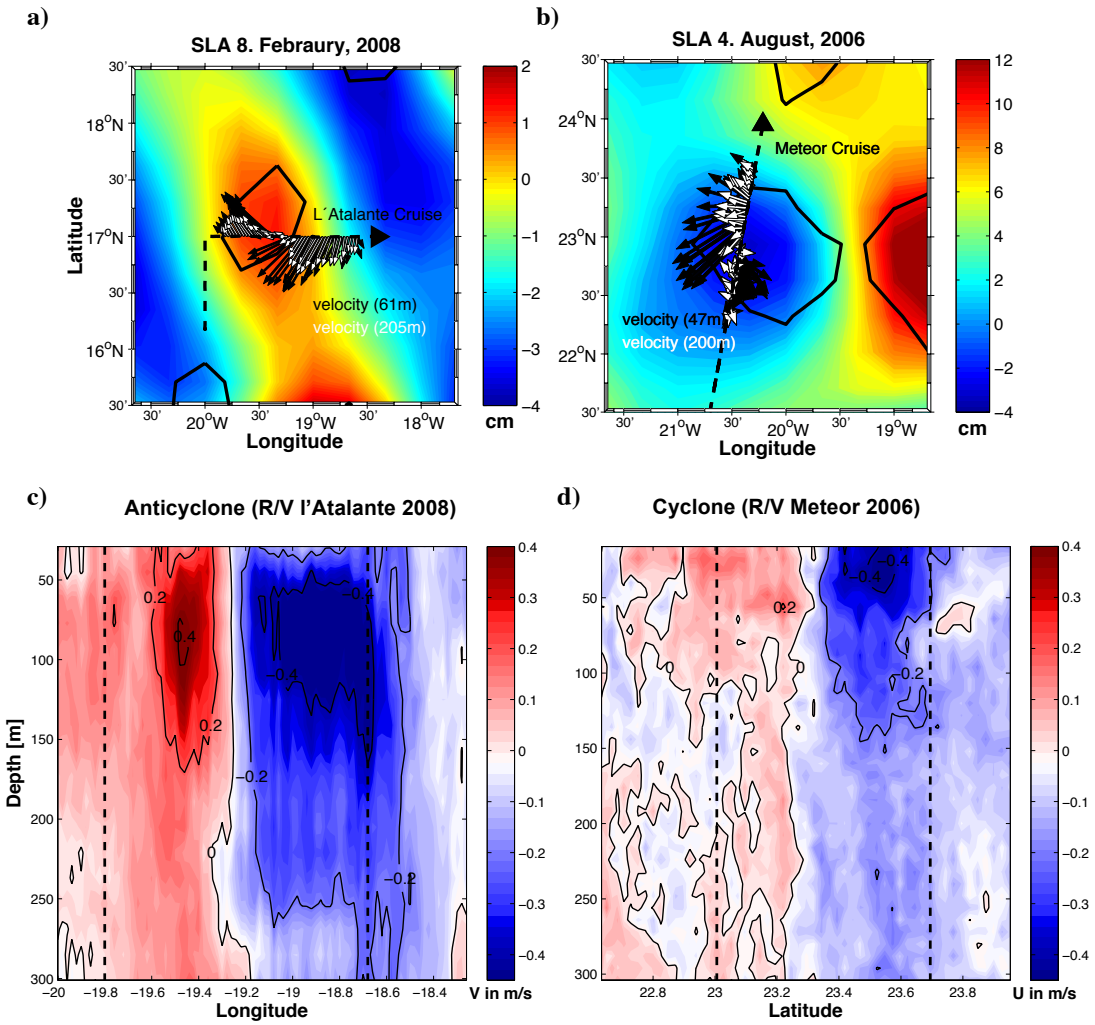

Figure 12: a) SLA of the 08.02.2008 (colour) superimposed with the l'Atalante cruise track (dashed arrow) and the SADCP measurements in 61m depth (black arrows) and 205m depth (white arrows), the black circle are eddies detected with the Eddie-Tracking-Algorithm **b)** The same for 04.08.2006 and the Meteor cruise track with SADCP measurements in 47m (black arrows) and 200m (white arrows) **c)** SADCP measurements from the l'Atalante during the crossing of the anticyclone, the dashed lines mark the radius detected from the Algorithm **d)** SADCP measurements from the Meteor crossing a cyclone.

Figure 12c shows the vertical profile of the velocities from the surface to a depth of 300m. The ship's ADCP measurements in Figure 12c) show first northward and then southward velocities (anticyclonic rotation), with a maximum azimuthal velocity of ± 0.5m/s in 80m depth. This is described as the core of an eddy. The velocities beneath 80m decrease again, but the structure is still clearly seen at a depth of 200m (Figure 12a) and 300m, the lower part of the measurement area of the SADCP. Structures like this are called anticyclonic mode water eddies (ACME), with velocity maxima under the surface and lower velocities at the surface [Karstensen et al. (submitted work)]. The size and radius of the eddy calculated from the tracking algorithm are presented in Figure 12a) and c) as well. In Figure 12c) the radius of the anticyclonic eddy, computed from the Eddie-Tracking-Algorithm of 39km from the eddy

centre (velocity is zero) is marked with the dashed lines.
Figure 12b) and d) show in comparison to Figure 12a) and c) a cyclonic rotating eddy structure. R/V Meteor crossed this structure on the 4. August 2006 on its cruise M 68/3. The cruise track, represented again as the dashed line, crosses directly an area of negative SLA (blue shading in Figure 12b). The ship's ADCP measurements, represented as arrows in Figure 12b) (black arrow in 47m, white arrows in 200m depth) and in Figure 12c show first a westward and later an eastward velocity (cyclonic rotation). The signature is not as strong as the one from the anticyclonic structure and might be disturbed by a westward background flow (eastward velocities much stronger than westward velocities). However, the strongest azimuthal velocities are from 50m depth up to the surface, with an amplitude of westward velocities of ~0.2 m/s and eastward velocities of ~0.5 m/s. With greater depths the velocities decrease rapidly and below 130m the structure is no longer detectable. Structures like this are called surface intensified eddies and in this case a surface intensified cyclonic eddy. The black line in Figure 12b) surrounds the area of the eddy, detected by the algorithm. The radius calculated by the Eddie-Tracking-Algorithm of 60km is also plotted in the SADCP measurements in Figure 12d).

Since the cruises were not carried out to resolve eddy structures by station measurements the available CTD data has a very low sampling rate, not able to resolve the horizontal eddy structure in detail. So to analyse the vertical temperature and salinity structures the sampling rate of mooring data with its local continuous measurements is preferred.

4.1.2 Vertical structure of temperature, salinity, oxygen and velocity (Example: ACME 2010)
At the end of February 2010 an ACME crossed the CVOO mooring, which is deployed about 60km northeast of the Cap Verde Islands (picture marked with a cross).
This event is studied by Karstensen et al. (submitted work) with regard to a low oxygen content within the ACME and therefore the importance to the marine life and the biogeochemical cycling. The following figure 13b), c) and d) are built after Karstensen et al. (submitted work).
The eddy came from the east and passed the mooring in a westward direction. Due to the high temporal resolution of temperature, salinity and velocity measurements at the mooring the vertical structure is well resolved and hence is presented as an example for vertical temperature, salinity and velocity section though an ACME (Figure 13).

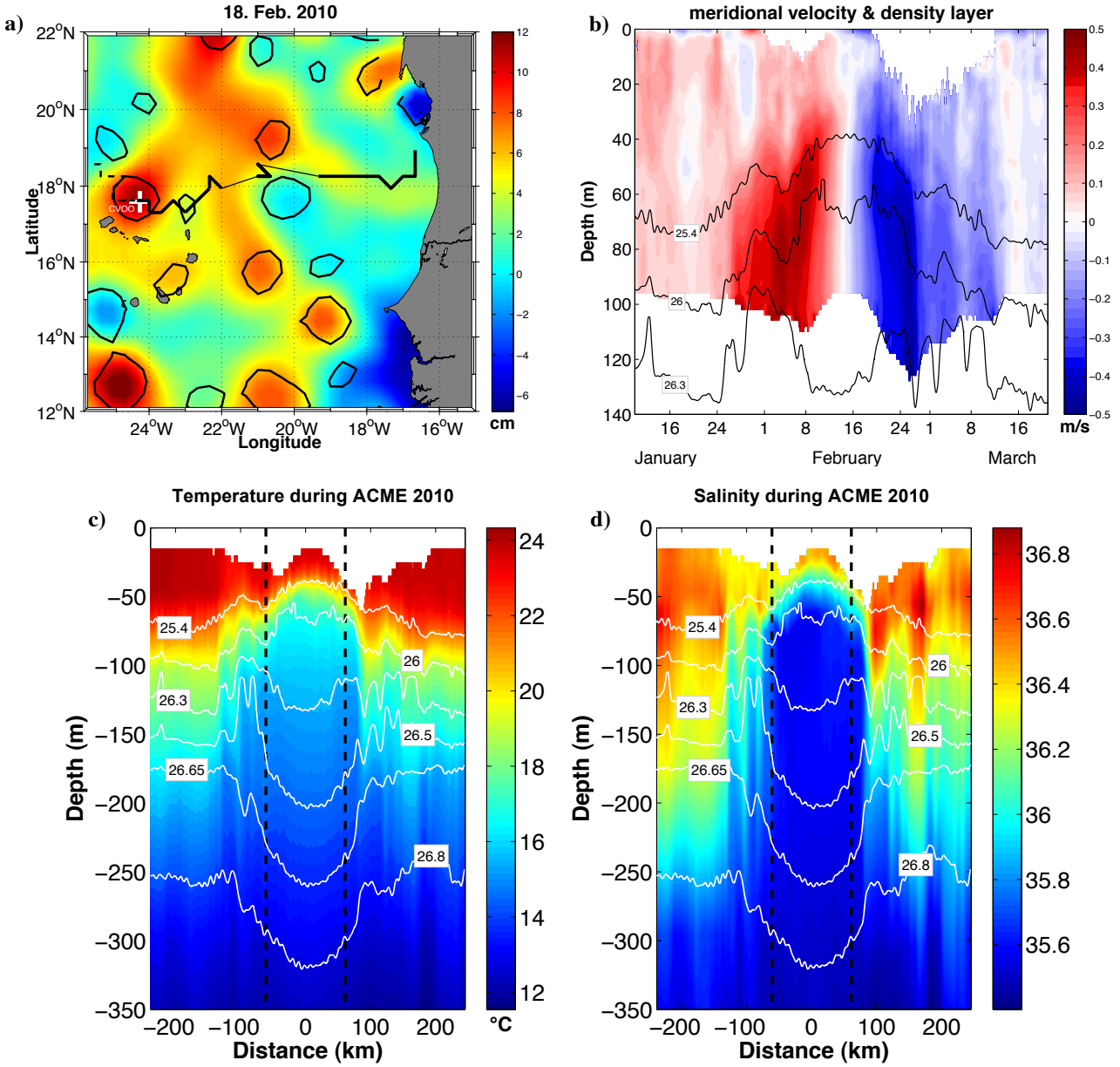

Figure 13: a) SLA of 18.02.2010 (colour) superimposed with the trajectory of the anticyclone which crosses the CVOO mooring in February 2010, the black circles are eddies detected with the Eddie-Tracking-Algorithm **b)** the ADCP measurements from the upper 140m of the CVOO mooring during the eddy crossing, superimposed with density layers (black contour) **c)** Temperature measurements from the upper 350m during the eddy superimposed are density layers (white contour), dashed lines indicate the radius computed from the Eddie-Tracking-Algorithm **d)** Salinity measured from the upper 350m during the eddy superimposed are density layers (white contour), dashed lines indicate the radius.

Figure 13a shows a snapshot of the SLA on 18.02.2010, which is about the date when the eddy centre crossed the CVOO mooring. The white cross indicates the moorings position and the black circle are the eddy areas detected by the algorithm. For that time a strong positive SLA is visible at the mooring position and the algorithm detected an anticyclonic eddy. The computed centre of the eddy was at 17°37.28N and 24°20.00'W and the mooring position is located at 17° 35.39'N and 24°15.12'W, which is a difference of only 9.1 km. Regarding the coarse 1/3° grid of the SLA data one could say that the eddy centre almost exactly passed the

mooring, as the eddy trajectory in Figure 13a shows. The continuous black line implies that the eddy was detected by the algorithm, whereas the thin line was a time when the algorithm 'lost' the eddy and it is was tracked visually. The dashed line is the way the eddy took after it left the mooring position. Figure 13b shows the velocities during the passage of the eddy, first strong northward velocities and later strong southward velocities, which stands for an anticyclonic rotation. The maximum azimuthal velocities are 0.7m/s at ~80m depth. The contour lines indicate density layers. The ACME is characterised by the velocity structure, with decreasing velocities towards the surface, and by the density structure, with the upward doming of the 26kg/m^3 isopycnal up to 50m and the downward bending of isopycnals in the deeper waters [Karstensen et al. (submitted work)]. This implies that the water within the eddy has almost the same density.

Figure 13c) and d) show the structures of temperature and salinity during the passage of the eddy. The white contour lines are the density layers and the vertical dashed black lines indicate the computed radius from the algorithm, which is 61km. It can be seen that the eddy contains colder and less saline water than the surrounding water. Following the 26.3kg/m^3 isopycnal the surrounding water has a temperature of ~18°C and a salinity of ~36.5, whereas the water within the eddy centre exhibit different water mass properties with a temperature of ~15°C and a salinity of ~35.5.

4.1.3 Changes and behaviour of an eddy during its lifetime (Example: ACME 2007)

To study the change in structure or behaviour of an eddy during its lifetime, it would be necessary to compare the eddy properties in an early state of the development, shortly after his generation, to the properties, in a later state of the development.

In February 2007 a similar ACME, like are discussed in *4.1.2*, crossed the CVOO mooring and is visible in all measurements (Figure 16 and 17). Seven days before the ACME went through the mooring position the R/V Poseidon on its cruise 348 at the position 17° 30'00N and 24° 00'00W crossed the same eddy, this gives us the chance to compare these two independent measurements. During the visual tracking of the eddy and the searching of eddy events in the ship's ADCP records it points out that also the Meteor, on its cruise 68/3, seven months earlier crossed exactly the same eddy close to its generation region, off Mauretania (Figure 16 and 17). This is certainly a good case to study the changes in the vertical structure of one eddy during its lifetime.

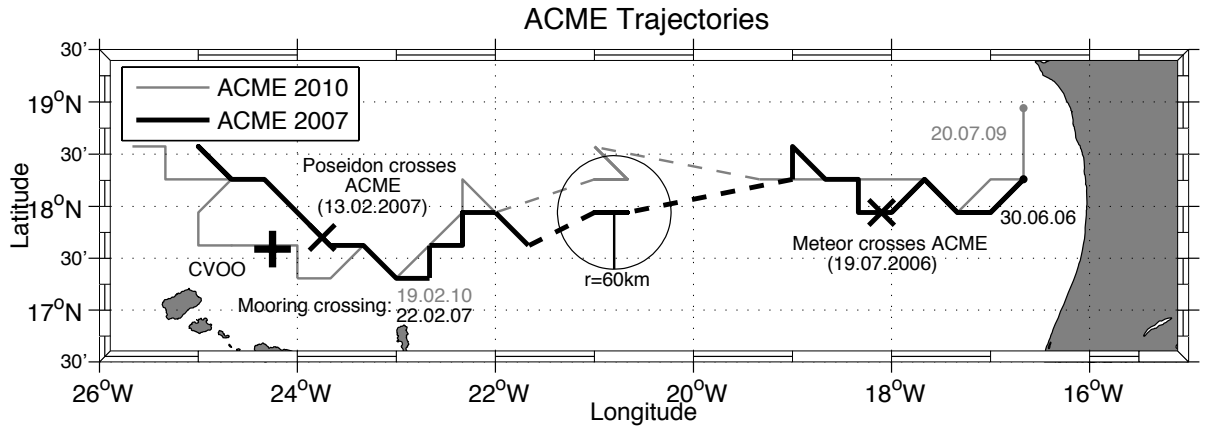

Figure 14: Trajectories from the two ACME's 2007 (black line) and 2010 (grey line), which cross the CVOO mooring (horizontal, bold cross), dates of the mooring crossing are given. The X marks the position where a research ship crossed the eddy. The point and date mark the place and time of the first detection by the algorithm. The dashed line mark the area the algorithm 'lost' the eddy. The circle shows the mean size and radius (60km) computed from the algorithm.

Figure 14 shows the pathways of the two ACMEs, which travelled through the CVOO mooring. The grey line is the eddy in the year 2010 (properties Figure 13) and the black line the one in 2007 (properties Figures 16 and 17). The place of the first detection is presented by a dot and the date is attached. Crosses mark the crossings from the R/V Meteor (19.07.2006) and R/V Poseidon (13.02.2007). A dashed line means that the Eddie-Tracking-Algorithm is 'losing' the eddy and it is tracked visually. The mooring position CVOO is also marked and attached with the associated date of the crossing. One can see that the ACME in 2007 does not pass the mooring position as central as the ACME in 2010 and therefore it is only captured an edge of the eddy, see the trajectory in Figure 14 or compare the SLA or relative vorticity field of Figure 11, which represent a snapshot of the day the eddy was nearest to the CVOO mooring. The R/V Poseidon cruise before did also not cross the eddy in its centre, whereas the R/V Meteor did.

The circle represents an area of ~11 600 km^2, which is the area of the ACME 2007 with a radius of 60.82 ±10.24 km when it is crossing the CVOO mooring position, computed with the Eddy- Tracking-Algorithm (see Figure 15). The size of the ACME 2010 on that position was ~11 500 km^2 with a radius of 60.62 ±12.87 km. The ACME 2007 was propagating westward with 0.97°/per month or 3.4 km/day and the ACME 2010 nearly with the same velocity of 1.07°/per month or 3.8 km/day. The mean radius from the ACME 2007 over his detectable lifetime was 46.65 km with a standard derivation of ±10.24 km. This order of magnitude is comparable with the ACME 2010 with a mean radius of 52.44 ±12.87 km. Generally the two eddies seem to be very similar. Note that they were generated on similar times in the year, at the same position and that they crossed the mooring nearly on the same

time in the year. Also the time and place where the Eddy-Tracking-Algorithm 'loses' the eddies is very similar.

To study the change during the lifetime of the ACME 2007 some results from the Eddy-Tracking-Algorithm during the time it has identified the eddy is shown in Figure 15.

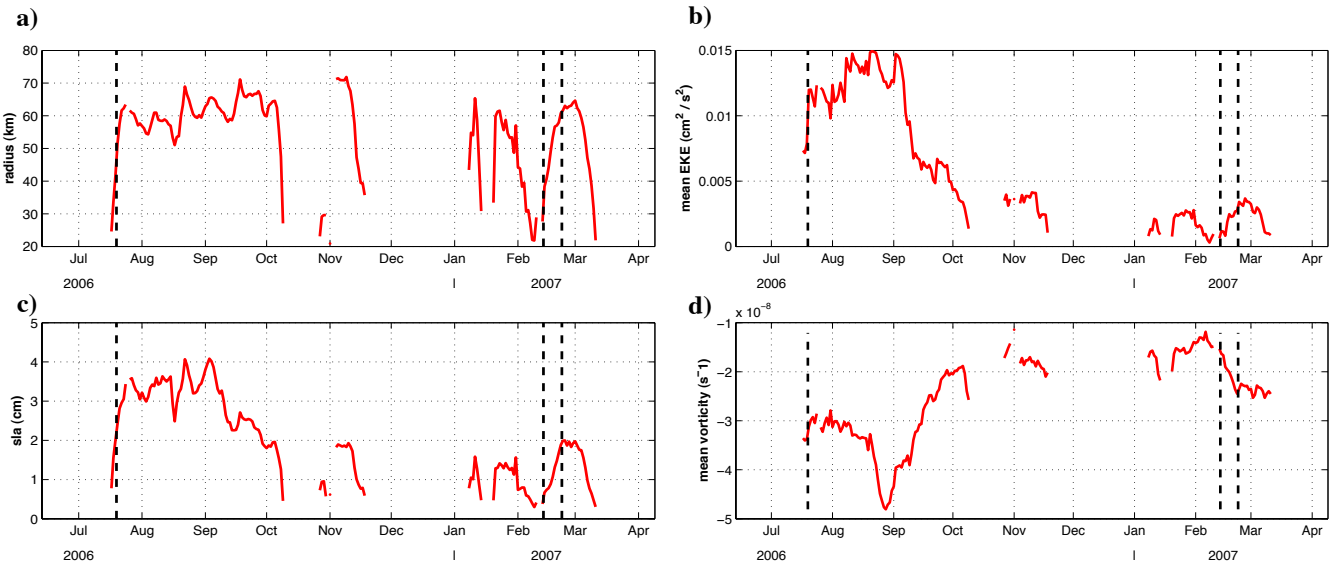

Figure 15: The **a)** radius in km, **b)** mean EKE in cm^2/s^2, **c)** SLA in cm and **d)** mean vorticity in 1/s from the ACME 2007 during its lifetime computed with the Eddy-Tracking-Algorithm. The dashed lines indicate the R/V Meteor, R/V Poseidon or the CVOO mooring measured the ACME.

The data gaps in Figure 15 correspond to the time when the Eddy-Tracking-Algorithm loses the eddy. The dashed lines indicate the time the eddy is meeting a research vessel or mooring. Figure 15 a shows the computed radius of the eddy and during the first tracking period, until October 2006, a constant increase from ~60 km (end of June) to ~70 km (end of September) is detectable. Some regular variability (~14 days) is detectable overlying this trend. But these phenomena are not detectable in the second tracking period from January to March 2007, during the mooring passage of the eddy the radius is ~60 km, comparable to its early development state.

The SLA magnitude (Figure 15c) shows a decrease from about 4 cm in the first tracking period to 2 cm or less during the time it crosses the mooring position. The mean vorticity (Figure 15b) and mean EKE (Figure 15d) approach zero over time. This indicates that the eddy is losing azimuthal velocity and energy along the way.

To compare these results the vertical velocity structures from the ACME 2007 measured from the R/V Meteor on 19.07.2006, the R/V Poseidon on 13.02.2006 and from the CVOO mooring on 22.02.2007 are shown in Figure 16.

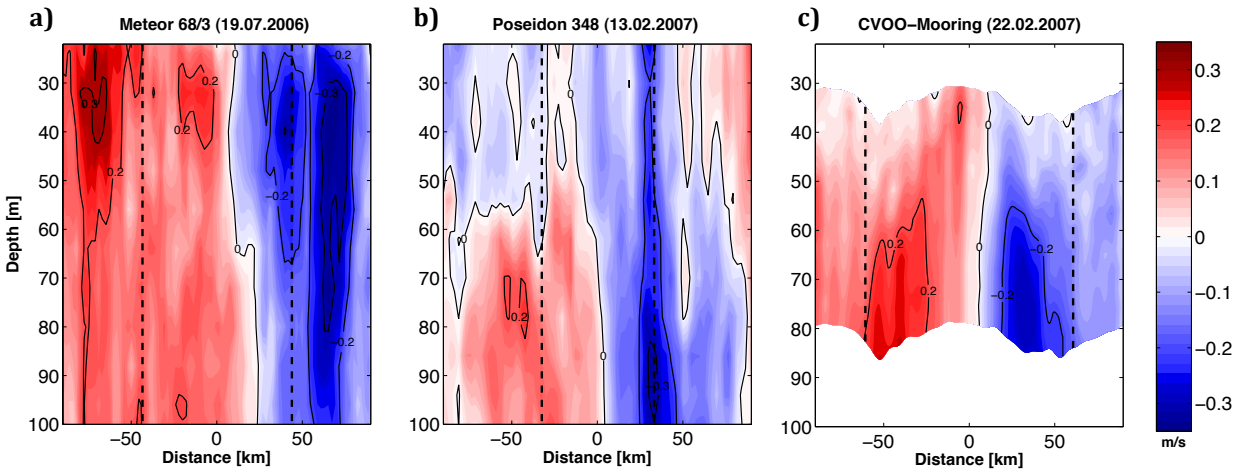

Figure 16: Meridional velocities from the ACME-2007 measured from the different ADCP's at different positions and different development states of the eddy. **a)** Meteor cruise 68/3 at position around 18°N 18°W (19.07.2006) **b)** Poseidon cruise 348 at position around 17° 30'00N 23° 59'00W (13.02.2007) **c)** CVOO-Mooring record from 08.02.2007 to 10.03.2007.

Figure 16a) shows the measured velocity from the SADCP of the R/V Meteor near the developing region along 18°N and between 17°W-19°W. Red shading is northward and blue southward flow. The vertical structure of horizontal velocity of Figure 16a) shows an anticyclone, with maximal radial velocity of ~0.4 m/s at depth of ~40m.

Figure 16b) and c) are the vertical structure of the meridional velocity from the same eddy seven months later. Figure 16b) is recorded from the SADPC on board of the R/V Poseidon from 17° 15'N and 25°W to 17° 30'N and 23°W and Figure 16c) shows the measurements from the CVOO mooring. The maximal radial velocities are at both measurements at a depth of ~75 m with an amplitude of ~0.3 m/s. Note that the vertical velocity structures from the later state of development, from Figure 16b) and c), and the density layers (shown in Figure 17a and b) point to an ACME with a core around ~75 m and the early measurements indicate the eddy core at ~40 m depth. This means the dynamic structure of the eddy has changed during its lifetime and its core has deepened from ~40 m to ~75 m depth.

The dashed lines indicate the radius of the eddy computed from the Eddy-Tracking-Algorithm at the day of the corresponding measurement. Out of Figure 15a) it can be seen that during the measurements of the R/V Meteor and R/V Poseidon the Eddy-Tracking-Algorithm newly detected the eddy and computed a small radius. More realistic is the radius ~60 km which is the average radius and also the computed radius during the mooring crossing, which goes well with all measurements.

To study the changes in the vertical structure of temperature, salinity and oxygen the five

CTD stations along 18°N at 19°W, 18.5°W, 18°W, 17.5°W and 17°W within the eddy event during the 18°N section from the Meteor cruise 68/3, are compared to the mooring measurements, seven months later (Figure 17 and 18).

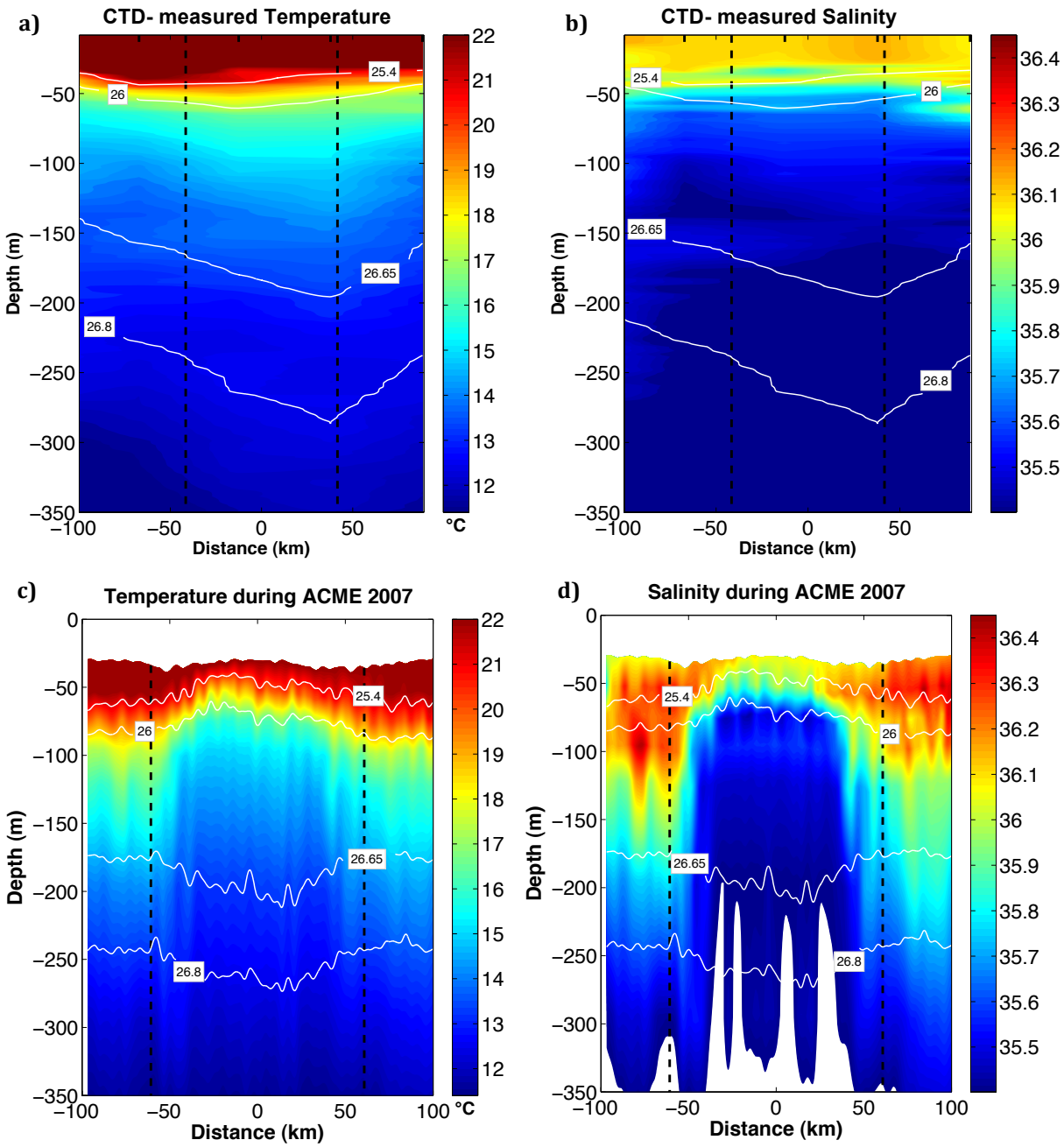

Figure 17: Vertical structure of temperature and salinity measured after the generation of the ACME 2007 and seven months later. White contours are the density layers. Dashed black lines indicate the radius computed from the Eddy-Tracking-Algorithm. **a, b)** CTD measurements of temperature and salinity carried out by the Meteor cruise 68/3 at positions 18°N at 19°W, 18.5°W, 18°W, 17.5°W and 17°W along 18°N, CTD-casts 30, 31, 32, 33 and 34 respectively. Positions are marked on the upper x-axis **c, d)** Temperature and salinity measurements from the CVOO mooring during the eddy event (08.02.2007-10.03.2007).

Figure 17 shows the vertical structure of temperature and salinity, superimposed with the contour lines of potential density, from the same eddy, Figure 17a) and b) at around 18°N

18°W and Figure 17c) and d) seven months and around 670km later at 17°35'N, 24°15'W. The dashed black lines indicate the radius of the eddy computed by the Eddy-Tracking-Algorithm. In the CTD-section (Figure 17a and b) it helps to identify the region of the eddy, because the temperature and salinity measurements are horizontally quite homogenous, in contrast to the eddy signal in Figure 17c) and c) is quite strong and well visible. The core properties deviate more strongly from ambient water masses in the later state (Figure 17c and d) compared to the earlier state close to the coast of Mauretania (Figure 17a and b). To compare these different water masses some temperature and salinity measurements along isopycnals before, during and after the eddy are selected. During the first measurement from the R/V Meteor at the 26kg/m^3 isopycnal a temperature of ~16°C and a salinity of ~35.7 prevail before, during and after the eddy. At the mooring position the surrounding water has a temperature of ~18°C and a salinity of ~36.4 along the 26kg/m^3 isopycnal and the water within the eddy centre exhibit a temperature of ~15°C and a salinity of ~35.5. Note that the water mass within the eddy centre at the mooring position has nearly the same water mass properties as the water, measured from the R/V Meteor near the coast of Mauritania. The surrounding water mass at the mooring position is a different water mass. This is also transferrable to the water mass properties of the ACME 2010 (see Figure 13).

To compare the oxygen content of the eddy at two different states of development the oxygen measurements carried out from the Meteor cruise 68/3 (Figure 18a) and the oxygen measurements from the CVOO mooring (Figure 18b) are compared.

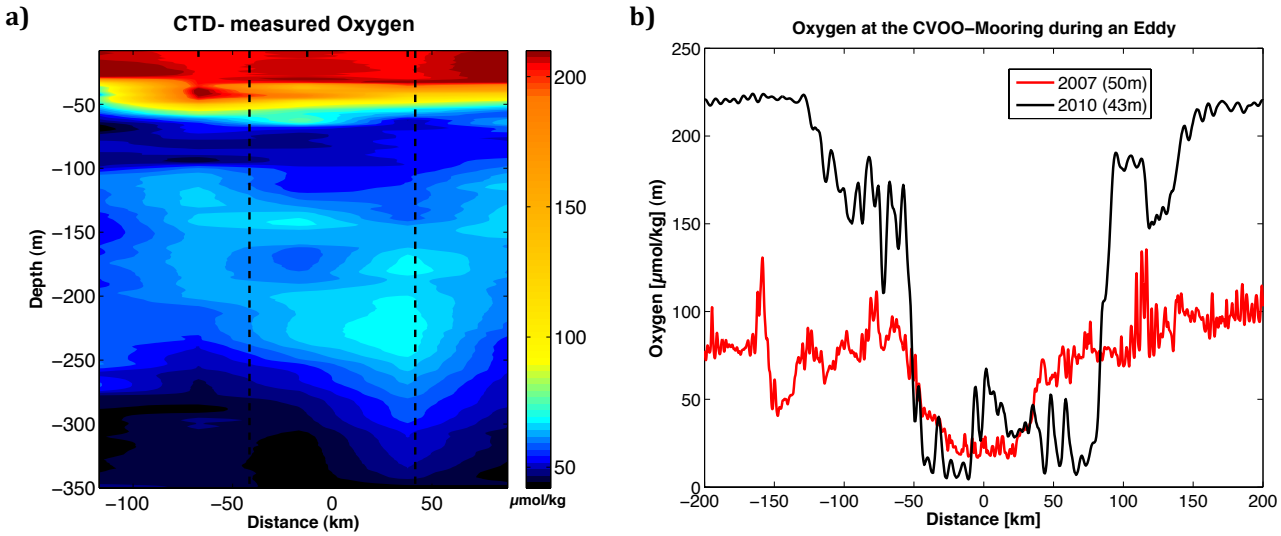

Figure 18: Oxygen measurements during the ACME 2007: **a)** Carried out by the Meteor cruise 68/3 around the 19.07.2006, black lines indicates the radius of the eddy and the ticks at the upper x-axis the CTD-cast positions and **b)** from the CVOO mooring at a depth of 50m (2007) and 43m (2010).

Figure 18a) shows the oxygen distribution during the ACME 2007 eddy event from 0-400m depths carried out from five CTD stations on the 18°N section. The dashed lines indicate the radius of the eddy, as it is detected from the Eddy-Tracking-Algorithm. The positions of the CTD stations are marked in black ticks on the upper x-axis. The vertical distribution of oxygen through the eddy seems to be very homogenous. No big difference is detectable, also regarding 50 m depths beneath the mixed layer.

In contrast the oxygen measurements during an ACME eddy event at the CVOO mooring (Figure 18b) show a notable out of the time series with very low oxygen concentration under the mixed layer. In the year 2010 with oxygen concentrations below 6 µmol/kg and 2007 below 20 µmol/kg, which is very low comparable to the oxygen content of the water before or after the eddy with 225 µmol/kg and ~100 µmol/kg, respectively for the eddy 2007 and 2010. The oxygen measuring optode at the CVOO mooring was located at a depth of around 43m in 2007 and at around 50m in 2010. But it must be kept in mind that the mooring experiences a vertical displacement during the eddy event due to the strong water velocities.

Figure 19 is created to illustrate the comparison of different properties computed from the Eddy-Tracking-Algorithm during a lifetime of an anticyclone and a cyclone. The anticyclone (red) was continuously tracked over a period of 200 days and the cyclone (blue) over 178 days.

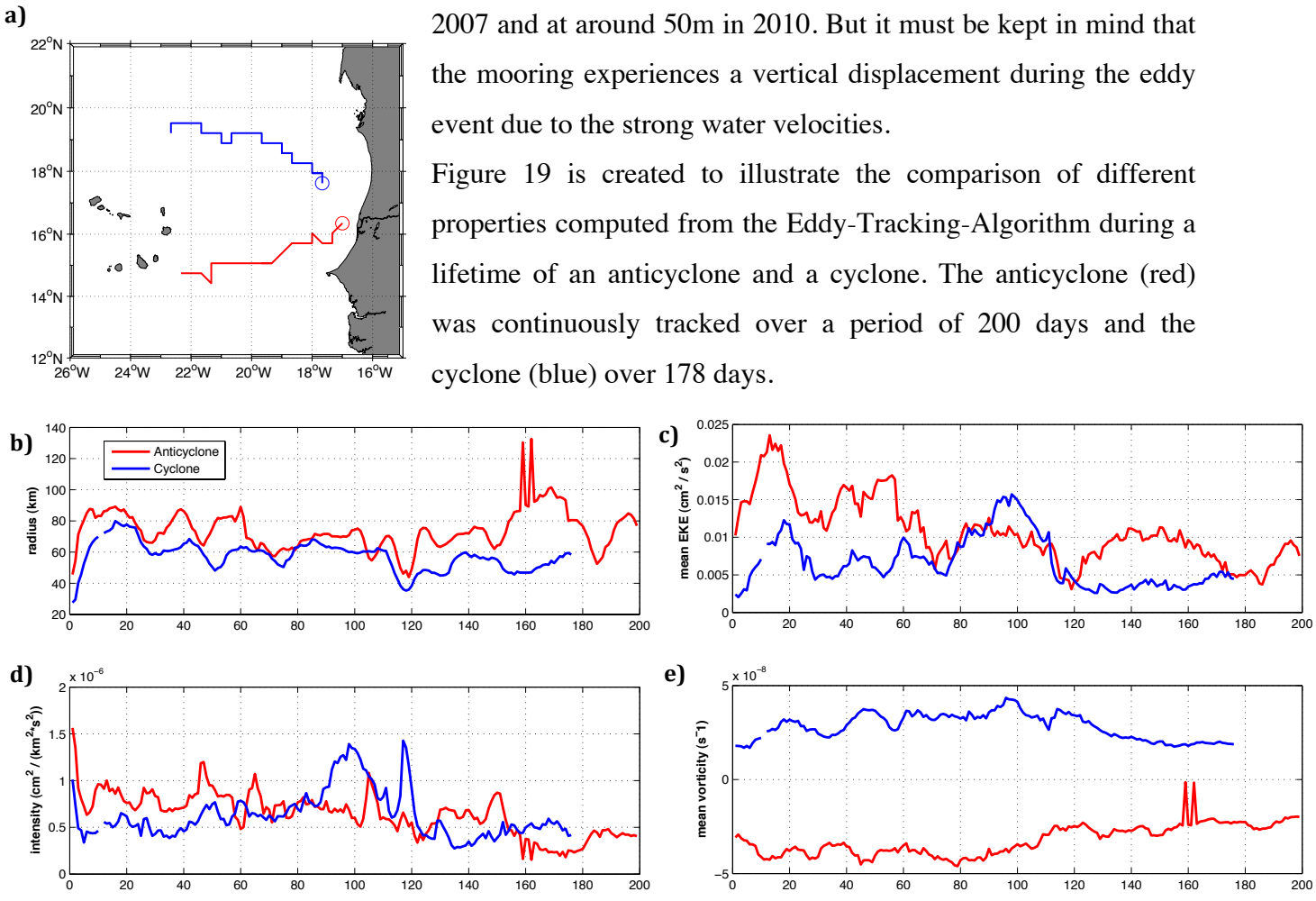

Figure 19: Two examples long tracked eddies, an anticyclone (red) and cyclone (blue).
a) Map including the pathways of the eddies.
b) Radius **c)** mean EKE **d)** intensity and **e)** mean vorticity against the time span in days they were tracked.

Figure 19a) shows a map of the pathways of the selected anticyclone and cyclone. The anticyclone has a meridional deflection to the south, whereas the cyclone is deflected to the north.

Figure 19b) shows their mean EKE which decreases with time, the anticyclone stronger than the cyclone. The radius in Figure 19c), shows a somewhat regular variability of about ~14 days from both eddies. Such behaviour was also detectable in the radius from the ACME 2007 (Figure 15a). The mean vorticity (Figure 19d) and intensity (Figure 19e) approach zero over time.

4.4 General eddy activity, its origin and distribution

To integrate the results of a single eddy event, its structure and behaviour, in a bigger context, a study of the results of the Eddy-Tracking-Algorithm is undertaken. The Eddy-Tracking-Algorithm takes the whole area into account and counts, tracks and identifies every single eddy, which occurred between 2000 and 2011 and had a radius >30km. This leads to an overview of all the eddy activity occurring in the upwelling area off Mauretania, which is described in *4.4.1 General statistics*. In addition the Eddy-Tracking-Algorithm provides indications of possible generating places, mechanism and about the general eddy expansion, which is described in *4.4.2 Generating places, 4.4.3 Indications of possible generating mechanism* and *4.4.4 General eddy expansion corridors*, respectively.

4.4.1 General statistics

In the upwelling area off Mauretania the Eddie-Tracking-Algorithm detects on average 92 ±9 new eddies per year (Table 4). They are subdivided into 55 ±9 anticyclones and 37 ±10 cyclonic eddies and in average mesoscale variability covers 15 % of the tropical northeast Atlantic. It must be kept in mind that these and all following numbers are based on all eddies which are visible for one week or longer and have a radius >30km. Table 4 gives an idea of the mean behaviour and shape of all the detected anticyclonic and cyclonic eddies in the region between 12°N - 22°N and 16°W – 26°W. The standard derivation of the values, which shows the variation from the average, is denoted in brackets.

Property	**All eddies (STD)**	**Anticyclones (STD)**	**Cyclones (STD)**
Total newly detected eddies	1009	600	409
Newly detected eddies [1/year]	92 (±9)	55 (±9)	37 (±10)
Newly detected eddies in the coastal area [1/year]	17 (±5)	10 (±3)	7 (±3)
Average lifetime [days]	39 (±35)	40 (±38)	37 (±33)
Average radius [km]	59 (±17.02)	60 (±17.32)	58 (±16.21)
Average area [km^2]	11 944 (±6 993)	12 314 (±7 337)	11 573 (±6 477)
Average SLA amplitude [cm]	-	1.76 (±1.52)	-1.61 (±1.16)
Average mean EKE [cm^2/s^2]	0.0075 (±0.0013)	0.0078 (±0.0013)	0.0072 (±0.0014)
Average westward propagation [km/d]	3.11 (±1.2)	3.54 (±1.32)	2.68 (±0.9)

Table 4: Mean properties of all eddies, anticyclones and cyclones in the region of 12°N - 22°N , 16°W – 26°W, detecable longer than one week and with a radius >30km.

Over all the years between 2000 and 2011 the Eddie-Tracking-Algorithm counted 1009 different eddies in the region of the tropical northeast Atlantic. The anticyclones tend to have a predominance with 600 detected anticyclones to 409 detected cyclones. The average radius and area of anticyclones and cyclones are of similar size, both of them varying much from one eddy to another. Also the modulus of the SLA amplitude, the mean EKE and the mean westward propagation are in order of the same size for both anticyclones and cyclones. All the values seem to have a great variability from one eddy to another, because the deviation around the average is always quite high.

Figure 20 shows the amount of eddies against the time span they were tracked from the Eddie-Tracking-Algorithm. It indicates that most of the eddies were only tracked over the time span of a week or two and that the amount of eddies decreases logarithmic with increasing time span. Between the years 2000 and 2011 ten anticyclones are quite robust and were detectable over a very long time (>150 days) and distance. Only one cyclone was detectable over 150 days or longer. The predominance of anticyclones is also visible in Figure 20, in which the anticyclones illustrates larger groups of eddies at every time span.

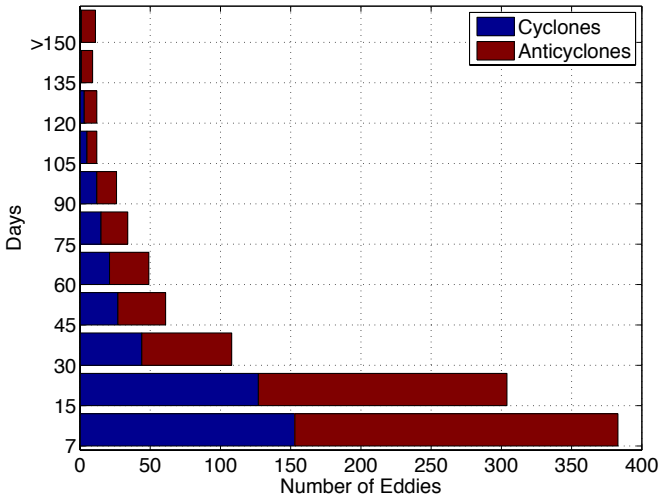

Figure 20: Number of eddies against the time span they could be tracked

4.4.2 Generation places

To identify the possible generating places of the eddies the location of the first detection of each eddy is counted in 1°x1° boxes to get a spatial distribution (Figure 21). It must be kept in mind, during the interpretation of the following figures, that a newly detected eddy from the Eddie-Tracking-Algorithm must not conclusively be a completely new eddy. This problem will be discussed later. However, Figure 21 is separated into a spatial distribution of all newly detected eddies (Figure 21a) and a subdivision into newly detected anticyclones (Figure 21b) and newly detected cyclones (Figure 21d).

A result of the distribution of Figure 21a is that it is evident that the most eddies are newly detected near the coast. In particular, with 30 newly detected eddies between 2000 and 2011 off Cape Nouamghar (Mauretania) in the box 19°N-20°N, 16°W-17°W, that will be referred

to in the following if Cape Nouamghar is discussed as a generating place. Also 30 newly detected eddies were counted in the box between 15°N-16N and 17°W-18°W north of Cap Vert (Senegal). The third spot is in the box between 16°N-17°N and 16°W-17°W off Saint Luis (Senegal) with 29 counts of new detections. In these three locations about nine newly detected eddies were counted per year.

Another slight increase of the values are detectable around 60 km off the Cap Verde Islands with 21 new detections. Also 21 new detections were counted northeast and southwest of the sea gate between Santo Antao and Sao Vincente, the most northern islands of the Cap Verde Islands (Figure 21a).

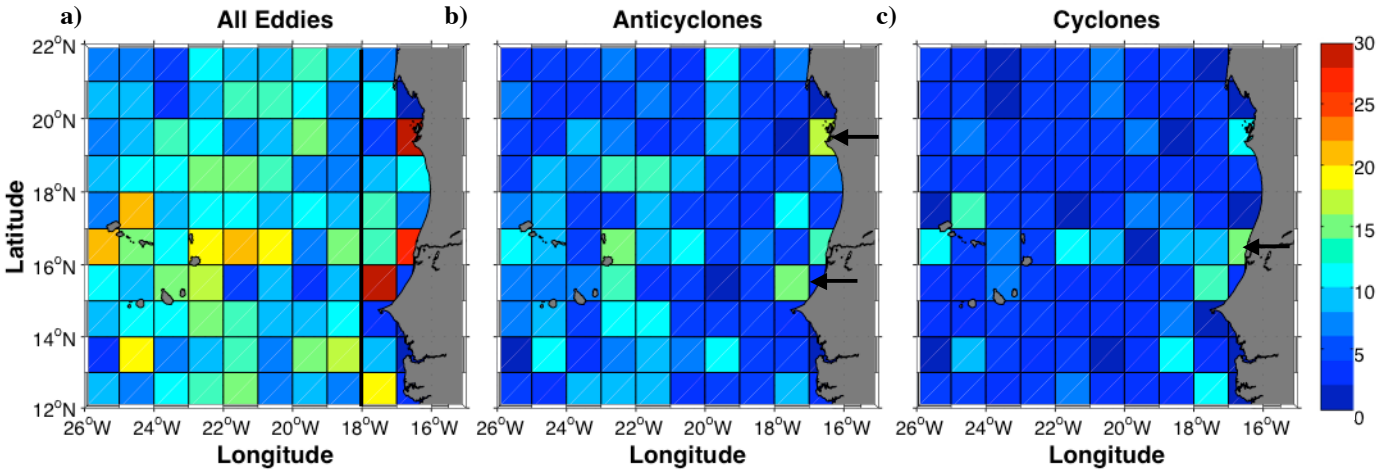

Figure 21: Spatial distribution of eddy generating places. A) All eddies b) Anticyclones and c) Cyclones. Arrows mark the three most productive generating places and the vertical black line along 18°W in a) separates the region into a coastal and offshore region.

The separation into anticyclones and cyclones in Figure 21b) and c) respectively, shows that anticyclones are most formed in the box off Cape Nouamghar (19 eddies) and north of Cap Vert (18 eddies), marked with an arrow in Figure 21b, whereas cyclones occur less in those places and more in the box off Saint Luis (19 eddies), also marked with an arrow in Figure 21c. Near the islands of Santo Antao and Sao Vincente anticyclones are created southwest of the sea gate and cyclones northeast of it. A higher production of anticyclones is also detectable east of Sal and Boa Vista in the box between 16°N-17°N and 22°W-23°W and from cyclones one box further east around 60 km east of the Sal.

4.4.3 Indications of possible generating mechanisms

After the localisation of possible generating places the term of interest is now to identify the mechanisms of generation and to study the interanual variability of these possible mechanisms. The idea is to count the first detection of an eddy and hence to conclude on the

eddy generation activity. But as mentioned above that is not so easy, the problem being that the Eddie-Tracking-Algorithm sometimes 'loses' the eddies on its track, due to a non-existent SLA signature and retrieves it after some time. Every time it retrieves an eddy the algorithm counts a new detection. This error results in a too high number of generated eddies, which are not really generated but just retrieved. A good example can be seen in Figure 14, which shows the trajectories from the ACME 2007 and 2010. The algorithm lost them two times and retrieved them but saved them every time as a new eddy, giving three eddies for when there should be just one.

To avoid that kind of mistake, a coastal area is defined between the African coast and 18°W (see black line in Figure 21a), where the main generating points are located. The assumption is that within the coastal area the Eddy-Tracking-Algorithm will not lose and retrieve the same eddy.

The inter-annual variability of all newly detected eddies in the whole area are shown in Figure 22a. This is done to get an overview over the inter-annual variability of the eddy activity in the whole region. To get an indication of the inter-annual variability of the coastal generating of eddies in the area, the amount of newly detected eddies in the coastal area is plotted in Figure 22b.

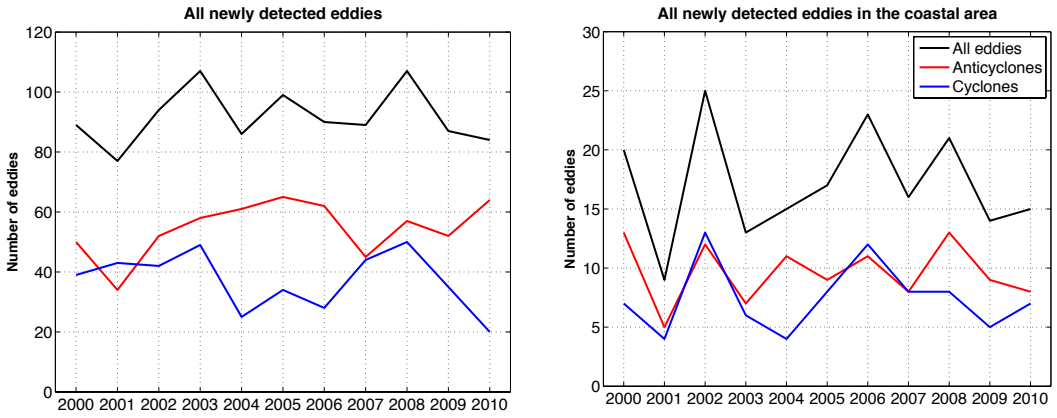

Figure 22: Number of newly detected eddies every year, the black line is the number of all eddies, the red the number of anticyclones and the blue from cyclones a) counted in the whole area b) counted in the coastal area.

In Figure 22a the black line indicates the amount of all newly detected eddies in the whole area (12°N-22°N to 16°W-26°W) and the red and blue lines are the number of all anticyclones and all cyclones counted in the area, respectively. The number of all detected eddies displays no large inter-annual variation. In two years, 2003 and 2008, a higher production rate of eddies (107 eddies) is detectable and in the year 2001 only 77 eddies are detected, this is 18% less than in the years 2003 and 2008. The separation into anticyclones

(red line) and cyclones (blue line) shows different patterns. It seems that there is a regular variability over a 6 year period, out of phase between the anticyclones and cyclones. In the year 2001, on the minimal turning point of the regular variability, only 31 anticyclones were detected, whereas in the year 2005, on the maximal turning point, 62 anticyclonic eddies were detected. The next minimum is reached 6 years after the last one in the year 2007 with a detection of 43 anticyclones. In contrast the most cyclones are detected in the year 2003 and 2008, with 43 and 46, respectively. The minimum is reached in the years 2004 with a detection of 23 cyclones.

Figure 22b) shows the amount of newly detected eddies in the coastal area. The black line indicates the number of all eddies generated and the blue and red lines represent the subdivision into cyclones and anticyclones, repectively. The variation of the amount of generated eddies is much higher, e.g. the lowest production rate is in the year 2001 with 9 eddies, whereas one year later 26 eddies are generated. The red line indicates that every second year (2000, 2002, 2004, 2006 and 2008) seem to be very productive in generating anticyclonic eddies, whereas the generation of cyclones peak in 2002 and 2006 with more production of cyclones then anticyclones.

To verify a possible generating mechanism a climatology of the first detections count in the coastal area is built (Figure 23). The climatology spans the years from 2000 to 2010 and shows the total amount of newly detected eddies per month over all years.

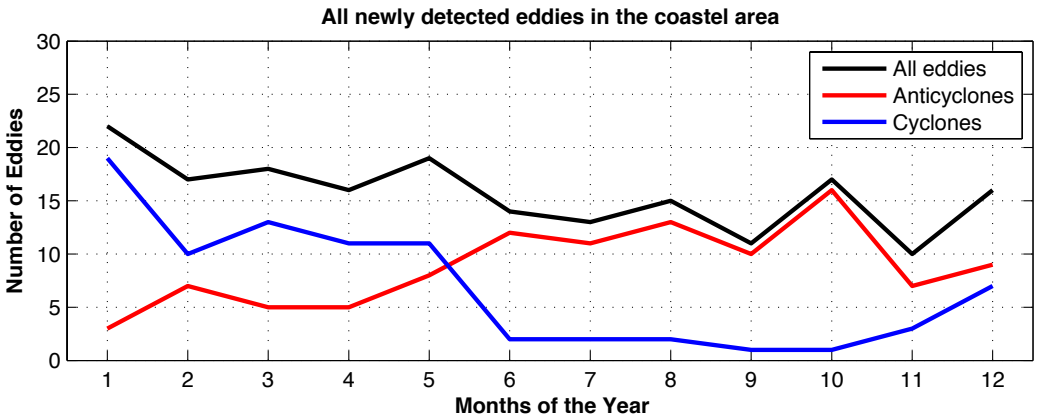

Figure 23: Separation of the number of newly detected eddies count in the coastal area over all years into months.

The black line indicates the total number of eddies, anticyclones (red line) and cyclones (blue line) are counted together. The most eddies are generated in boreal winter, especially in January (22) after which the amount of eddies generated decreases slowly over the year. A very clear seasonal cycle in the production of all eddies is not obvious. In contrast to this the

separation into anticyclones and cyclones shows a clear annual pattern. The large amount of eddies generated in January for example is nearly covered by the production of cyclones, 19 cyclones are created in comparison to 3 anticyclones. In contrast the production of eddies in late boreal summer is dominated by the production of anticyclones. In eleven years only 2 cyclones occurred in the months of September and October.

4.4.4 General eddy expansion corridors

To verify possible distribution pathways a count was made of how many eddies, which were tracked without disturbance for longer than 3 months, are in 1/3° grid boxes every day. Every eddy could only count ones. This leads to a distribution of eddy activity, which is plotted in Figure 24 and represented as the red and yellow colour. Red colour indicates high eddy activity and white low. The dataset is interpolated on high resolution 1/20° grid, so the colours indicates eddies per 1/20° grid box. Unfortunately, the eddy activity gives no information about the direction of eddies, therefore eddy trajectories are superimposed of eddies, which are tracked without disturbance over five months (140 days) or longer. The circles represent the place, where the eddy was detected for the first time.

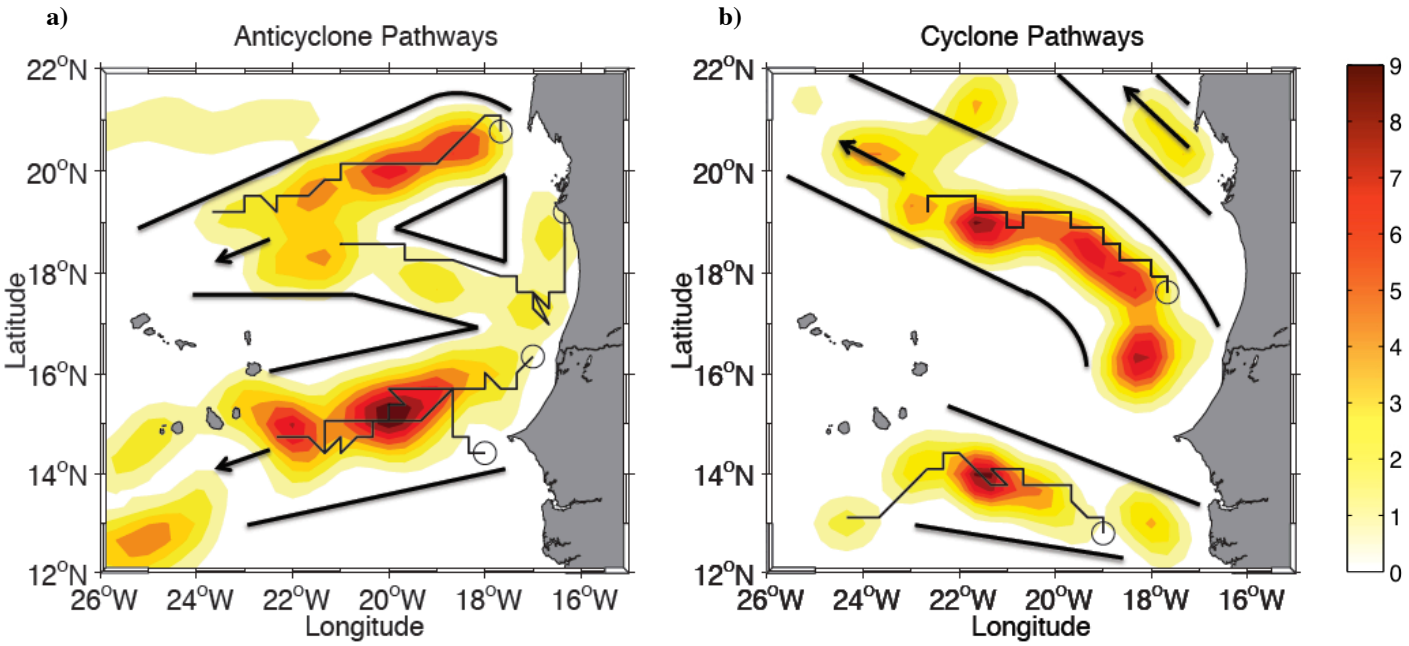

Figure 24: Pathways superimposed with trajectories and corridors from **a)** anticyclones and **b**) cyclones.

The black corridors and the black arrows are the corridors and directions, which most of the eddies take on their westward way from the generating places near the coast into the ocean. Figure 24a) shows the pathways of the anticyclones, whereas Figure 24b) indicates the

pathways of the cyclonic eddies. The source regions near the coast are detectable in both figures and from there all eddies tend to move westward away from the coast into the open ocean. The anticyclones (Figure 24a) tend to have a stronger southward component within their pathways and the cyclones (Figure 24b) show a tendency to a stronger northward component.

5. Interpretation

The interpretation of the results is divided into two parts. In the first part the examination of single eddy events is interpreted and discussed, with regard to the dynamical vertical structure, the vertical temperature, the salinity structure and the changes of an eddy during its lifetime as illustrated by the example of the ACME 2007.
The second part consists of interpreting the results from the Eddy-Tracking-Algorithm to characterise the mesoscale variability within the region, interpret the main locations of origin and discuss possible generating mechanisms.

5.1 Single eddy events

During the visual search of eddy events from the ship ADCP measurements and the mooring ADCP time series, it becomes apparent that both cyclones and anticyclones appear in different horizontal shapes and vertical structures. Eddies were detectable in horizontal length scales of between 30km and 70km and maximum azimuthal velocities vary from slow rotation of 0.1m/s up to 0.8m/s. In the vertical the variation of structures was also evident, as some of the located eddy events are surface intensified eddies (like the chosen example cyclone in Figure 12d) and others have their maximum velocities between a depth of 30m to 100m. One exception was an eddy structure at a depth of 150 m (not shown) detected by the Poseidon cruise 348 in 2007, with maximum speeds at around 250 m, whereas between 0-150 m no rotating structure was visible.
Most of the detected structures were highly baroclinic eddy structures, e.g. the chosen cyclone in Figure 12d) with vanishing signature beneath a depth of 130 m. One exceptional eddy structure (not shown) carried out during the Meteor cruise 68/3 on 1st August 2006 had a continuous rotation over the whole water column, like a solid body rotation, from the surface to a depth of >800m. Unfortunately at this depth the range of the SADCP ended, so it cannot certainly be said that this is a barotropic structure, more realistic is to say that this is a low order baroclinic mode.

Taking the ACME 2010, which passed the mooring position in mid-February, as an example, the vertical temperature, salinity and velocity structure of an eddy will be discussed (Figure 13). The trajectory in Figure 13a) shows that the ACME 2010 was most likely generated off Cape Nouamghar, in the upwelling region off Mauretania during late boreal summer. From there the ACME 2010 started to travel westwards at a rate of 3.79 km/day, away from the

coast into the offshore ocean. At the generation place the ACME 2010 had a radius of ~60km and held this size more or less constantly on its way to the west along 18°N. At the mooring position the ACME 2010 had a maximal azimuthal velocity of 0.7m/s at a depth of ~80m in its core, which is quite strong compared to the ACME 2007 and the other observed eddy structures. The Rossby number, which is defined as:

$$Ro = \frac{V_m}{f \cdot R_m} \tag{9}$$

where V_m is the mean azimuthal velocity, R_m the mean radius and f the Coriolis parameter. For the ACME 2010 the Rossby number was 0.26, which is a common value for mesoscale eddies [Alpers et al. (2013)].

The change in temperature and salinity of the ACME 2010 is very apparent in Figure 13c) and d). It stands out that the eddy contains colder and less saline water than the surrounding water. The temperature and salinity properties of the investigated region as carried out by the Argo profiles are plotted in a T/S diagram in Figure 25. The salinity and temperature values following the 26.3kg/m^3 isopycnal from the surrounding water and the water inside of the eddy is marked with triangles. The purple triangle indicates water from the eddy core, whereas the green triangle indicates the surrounding water. One could see that the water from the eddy core equates to SACW and the surrounding water mass properties to NACW, which is warmer and has a higher salinity. The reason for this is that the eddy was generated within the upwelling area close to the coast, where the abundant water mass is SACW. It transported this water, captured in its core, to the mooring position north of the Cap Verde Islands, which is north of the CVFZ, where the abundant water mass is NACW.

The eddy captures the SACW in its core because the translation velocity of the eddy (0.04 m/s) is much smaller than the rotation velocity (0.7 m/s). The rotation prevents the surrounding water from influencing the water in the eddy core.

Thanks to the multiple measurements that were carried out on the ACME 2007, this eddy is an especially good example on which to base a discussion of the development of an eddy during its lifetime. The trajectory in Figure 14 shows that it was most likely generated off Cape Nouamghar during late boreal summer, similar to the ACME 2010. It travels westward along 18°N with a propagation speed of 3.4 km/day (ACME 2010: 3.79km/day). In the following eight months the Eddy-Tracking-Algorithm 'lost' and retrieved the eddy two times, see Figure 14.

Figure 15 enables study of the changing ACME 2007 properties computed from the Eddy-Tracking-Algorithm. It can be seen that the ACME 2007 was more or less constant in its size during its lifetime. Between July and October, when the Eddy-Tracking-Algorithm worked

well, a regular ~14 day variability is detectable. Sangrá et al. (2005) follow with insitu measurements in the eastern subtropical Atlantic an anticyclone and observed a similar pulsation of the radius. The observed periodicity was a couple of weeks, which agrees with the observed periodicity of the contraction and expansion of the radius from the ACME 2007. They related these pulses to different phases of maximum and minimum eddy eccentricity that develops in vortices [Sangrá et al. (2005)].

The amplitude of the SLA, the mean EKE and the mean vorticity of the ACME 2007 decrease over time, indicating a slowing rotation and a loss of energy. This is most likely due to the internal friction and dissipation, which is abundant throughout.

The lost of azimuthal velocity is also detectable in the different ADCP measurements. The first one was measured near the developing region, where a maximal azimuthal velocity of 0.4 m/s at depth of 40m was noted. The second measurement, taken seven months later, north of the Cap Verde Islands, recorded a maximal azimuthal velocity of 0.3 m/s at a depth of 75m (Figure 16c and d).

Studying the vertical velocity structures at different developing states of the ACME 2007 an interesting fact becomes obvious: The maximal velocities at ~40m depth at the earlier state of the eddy, migrate towards ~75m depth at a later state of the eddy (Figure 16). The reasons for the deepening of the eddy core during its lifetime of about 35m is not fully understood, but it might be an interesting fact to keep in mind for further research.

When it comes to temperature and salinity measurements of the CVOO mooring, there is again an indication, that SACW is transported within the eddy core into a region were NACW dominates. On this example it was possible to study the lateral mixing ratios of the two water masses within and around the eddy during its lifetime. Temperature and salinity measurements of the eddy core after its generation (Figure 17a and b) are compared to the temperature and salinity measurements from the eddy core at the mooring position (Figure 17c and d). The measurements from the CVOO mooring before and after the eddy crossing are averaged to calculate the surrounding water mass properties. So the stability of the eddy during its westward trajectory of 670km can be investigated (Figure 25b). For the stability analysis the temperature and salinity values are selected in steps of 0.05 kg/m^3 density between the 25.6 kg/m^3 and 26.65 kg/m^3 isopycnals. These densities are chosen in such a way that the analysis begins beneath the mixed layer, because diapycnal mixing must be disregarded, for more information see chapter *3.4 CVOO Mooring data*. It was assumed that the measurements from the Meteor 68/3 cruise capture the original SACW properties. The measurements from the mooring before and after the eddy crossing are used as the

surrounding water mass, the NACW. The measurements in the eddy core from the mooring during its crossing are assumed to be a mixture of the former two. The different salinity and temperature measurements along the mentioned isopycnals are plotted into a T/S diagram of Argo profilers (Figure 25). The black crosses labelled with '$SACW_{R/V\ Meteor}$' mark the water from the eddy core from its early development state. The blue stars labelled with '$Mix_{Mooring}$' indicate the water mass from the eddy core in its later development state and the red crosses labelled with '$NACW_{Mooring}$' indicate the surrounding water mass.

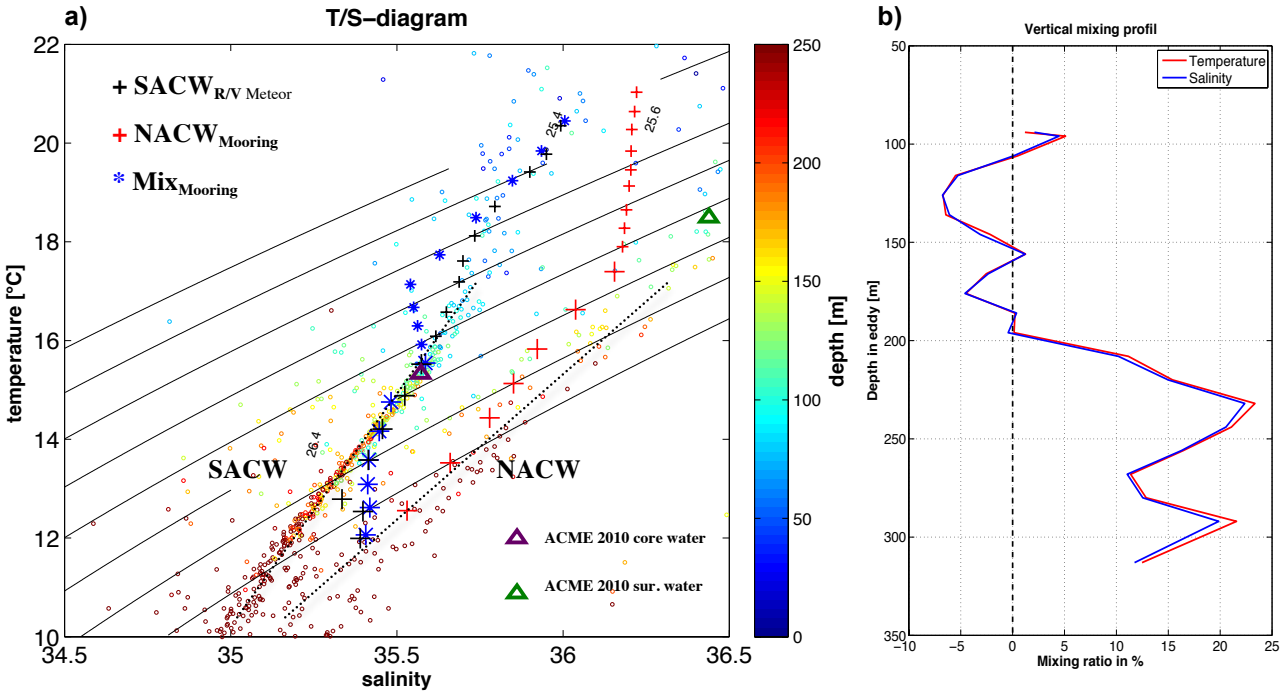

Figure 25: a) T/S diagram from Argo profiles superimposed are the potential density layer and the colour indicates the depth. Marked are water properties from the ACME 2007 surrounding water measured at the CVOO mooring (red crosses). The water mass properties from the ACME 2007 during its early state measured from the R/V Meteor (black crosses) and finally the water mass properties inside of the ACME 2007 at the CVOO mooring position (blue stars). Bigger markings indicate a temperature or salinity beneath the mixed layer. The purple triangle indicates the water inside the ACME 2010 and the green triangle the surrounding water from the ACME 2010 both at the 26.3kg/m^3 isopycnal. **b)** Vertical mixing profile showing the mixing ratios in % of temperature (blue) and salinity (red) from the NACW into the eddy core.

It stands out that all the measurements from within an eddy core consist of SACW (black cross, purple triangle and blue stars), whereas all the measurements of the surrounding water lie in the NACW area (red crosses, green triangle). The larger markings indicate that the measurement comes from below the mixed layer, whereas smaller markings indicate measurements from inside the mixed layer. Measurements from the eddy core during the two different times within the mixed layer vary (compare small blue stars and small black crosses). Less saline and colder water is coming into the eddy at a depth of ~50m, whereas towards the

surface the core properties become more similar again. This can be explained through phenomena including diapycnal mixing, which are difficult to discuss with the existing dataset. Interesting is that the temperature and salinity properties of the mixed water mass and the early core water mass properties beneath the mixed layer (bigger marking size) do not show large differences. This means the water mass properties in the core remained nearly unchanged during the 7 months of westward travel. An exception is one measurement at ~240 m depth (26.7 kg/m^3), which shows a stronger influence of SACW.

The lateral mixing ratios beneath the mixed layer of temperature and salinity are shown in Figure 25b). Very little lateral mixing appears in the eddy core at the depth beneath the mixed layer down to a depth of 200 m. The water mass in the eddy is very similar to what it was at its origin. With depth the lateral mixing increases due to the fact the influence of the eddy vanishes so that the water is no longer captured.

Also the ACME 2007 translation velocity (0.0394 m/s) is much smaller than the rotation velocity (0.3 m/s) as it was also the case for ACME 2010. So the assumption that the water is captured within the ACME 2010 as an enclosed system seems to be reasonable.

An aspect that has to be mentioned during the stability discussion is that the eddy was travelling within the influence of the SACW during a long period of time. So the assumption that the surrounding water mass consists of NACW all the time might be false. For a better analysis, information about the 'real' surrounding water masses for the complete time period ought ideally to have been known.

However the eddies in the tropical northeast Atlantic, generated at the coast, appear generally to transport cold, fresh and nutrient-rich SACW from the coast to the open ocean, over the CVFZ into a region were NACW dominates.

Comparing the oxygen contents it shows that during the early state of the eddy its signature in oxygen was not detectable. From the surface to a depth of 100m the horizontal distribution is homogenous and shows a normal pattern in the vertical, with very high oxygen at the surface and a strong decrease under the mixed layer into the upper oxygen minimum zone.

On contrary the oxygen measurements at the CVOO mooring (Figure 18b) are noticeably low under the mixed layer, with oxygen concentrations below 20 μmol/kg during the ACME 2007 and below 6 μmol/kg during the ACME 2010. The oxygen content before the eddy was 225 μmol/kg and 100 μmol/kg at that depth, for the ACME 2007 and 2010 respectively.

Oxygen is, compared to temperature and salinity, not a conserved water property because it can be consumed due to biological processes. This means that it is also an indicator that the

water within the eddy was captured along with the biological life, which consumed all the oxygen in its core during the lifetime of the eddy. This must have an impact on the marine life and the biogeochemical cycling within the eddy. As an example variations in the behaviour of the reflecting particles, which partly exist of zooplankton, could be observed in the backscatter of the ADCP. As the eddy passes they cease their normal daily migration from the deeper ocean during daylight to the mixed layer at night and remain in the deeper ocean because they do not want to go into waters with very low oxygen contents. For more information see Karstensen et al. (submitted work) who investigate these processes during an eddy passing in more detail.

5.2 Interpretation of the results from the Eddy-Tracking-Algorithm

To characterise the eddy activity in the tropical northeast Atlantic some averaged eddy properties are computed with the Eddy-Tracking-Algorithm (Table 4). The result is that on average 92 ±9 eddies exist in the region per year, subdivided into 55 ±9 anticyclones and 37 ±10 cyclones.

This number is certainly too high because of the mentioned problem of double counting, in chapter *4.4.3 Indications of possible generating mechanisms*. The reason for the disappearance of the SLA structure and the associated loss of the eddies from the Eddie-Tracking-Algorithm is not fully understood. One possibility could be the documented eddy pulsating as it travels westwards [Sangrá et al (2005)]. Figure 15 also indicates that there could be some kind of 14 day pulsation of an eddy, visible in the radius and SLA. But it is clearly noticeable that trajectories from some selected eddies, for example the ACME 2007 and 2010 in Figure 14, are disconnected in similar regions. If the disconnection happens in connection with the pulsation of the eddy it should follow a 14 day cycle, which is not observed in the study. Following the anticyclones built off Cape Nouamghar during late boreal summer on their westward way along 18°N, within the middle corridor from Figure 19, it appears that many of them are lost between 19°W and 21°W and retrieved again between 21°W to 24°W. This is also reflected as high eddy activity in Figure 19 and there are 16 new detections of anticyclones in the boxes 18N-19N 21W-22W and 18N-19N 22W-23W of Figure 16b. Apart from the coastal region these are the boxes containing the most newly detected anticyclones, located in the middle of the open ocean with no strong currents, seamounts or islands close by which might generate instabilities. Therefore the high number of new detections in the boxes must be due to the fact that the Eddie-Tracking-Algorithm is retrieving already counted eddies, there.

These well-defined areas where the eddy signature is getting lost could also possibly be explained due to wind anomalies, which hide the SLA signature [personal communication Johannes Karstensen]. Figure 21 shows the standard derivation of the wind stress for the year 2008 as an example, also marked are the boxes containing a high number of newly detected anticyclones. Following the eddy pathways along 18°N the boxes lie next to an area of high standard derivation of the wind stress (Figure 26). The mechanism of the connection between a wind burst and the disappearance of the eddy SLA signature is not completely understood so far. In this case it might be an interesting approach for further research studies to investigate the disappearance of the SLA signature, rather than the pulsating of eddies. However, this effect of the disappearing eddy SLA signature breaks the trajectories, underestimates the age of the eddy and, if the algorithm finds it again, over estimates the number of eddies in the region. These phenomena must be kept in mind when studying the Eddy-Tracking-Algorithm results.

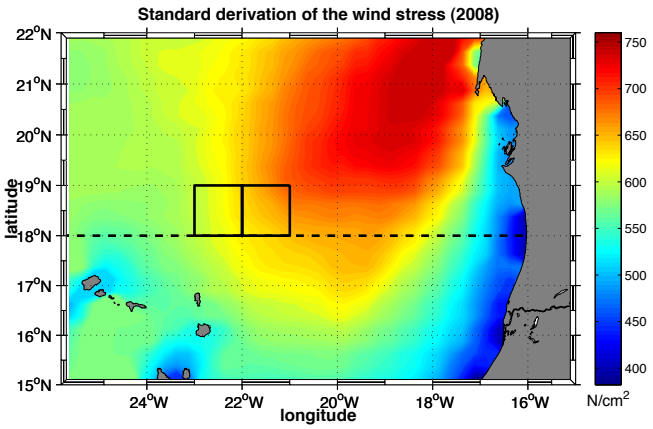

Figure 26: Standard derivation of the wind stress 2008. Superimposed boxes of high anticyclone new detections, compare figure 16b.

One result is that on average per day ~15 % of the area is covered with mesoscale variability. Chaigneau et al. (2008) computed that ~23% of tropical eastern South Pacific are covered with mesoscale variability, so this seems to be typical for an eastern boundary current region.

All detected eddies in the studied area had an average radius of 59km, whereas Chelton et al. (2011) computed a mean radius of ~90km, on that latitude band.

Furthermore the detected eddies were all travelling westwards, as to be expected from the β-drift theory, with an average travelling speed of 3.11km/day. This is in line with the typical phase speed of a baroclinic Rossby wave.

1009 eddies were counted between the years 2000 and 2011 subdivided into 600 anticyclones and 409 cyclones. This imbalance in favour of the anticyclones is found in other studies too, such as Chaigenau et al (2011) in the eastern south Pacific and Chelton (2007) in its global monitoring of mesoscale eddies. However this is not found in all studies, see Sangrá (2009) on the subtropical Atlantic and Chelton (2011) on global monitoring of mesoscale eddies.

In this work the eddies had an average lifetime of 39 ±35 days. It seems that anticyclones have a longer life expectancy and are more stable. This is also observed by Sangrá et al. (2009).

To avoid the error of double counting and still get indications of possible generating areas, a coastal area from the coast to 18°W is defined. It was not observed within this area that the Eddy-Tracking-Algorithm lost or retrieved eddies. So the number of newly detected eddies can be taken with more certainty as the amount of newly generated eddies. On average 17 ±5 eddies were built in the region subdivided into 10 ±3 anticyclones and 7 ±3 cyclones. Within the coastal region most eddies are generated off Cape Nouamghar (Mauretania), north of Cap Vert (Senegal) and off Saint Luis (Senegal), see Figure 16. It is conspicuous that they were generated around land tongues, which can be seen in connection with instabilities of the boundary currents, due to current deflection and friction. The fact that headlands all over the world are possible birthplaces of eddies is well known [e.g. Alpers et al. (2013)].

To get a better understanding of the generating mechanism of the anticyclones and cyclones a climatology of newly detected eddies was built within the defined costal area over the time span from 2000-2010 (Figure 27). In total most eddies are build in January with a slight decrease over the year, which is in agreement to similar studies in the tropical northeast Pacific [e.g. Liang et al. (2012)]. Liang et al. (2012) showed the mean standard derivation of high pass filtered SLA, as an indicator for mesoscale variability, averaged over the Tehuantepec region in the tropical northeast Pacific (Liang et al. (2012) Figure 7). This climatology exhibits the same annual cycle (most in January/February/March then decreasing with a slight peak in October/November/December). This holds true if we consider all detected eddies.

To identify the generating mechanism of the eddies a distinction between the seasonal cycle of cyclones and anticyclones is meaningful, which is shown in Figure 23. It is evident that the generation does not occur on a regular basis through the year. So it must have been caused by a change in environmental conditions around the headlands. Most anticyclones are generated in late summer/autumn and less in winter/spring and most cyclones are generated explicitly in January and less in summer/autumn.

The generating places of anticyclones and cyclones showed that they were both probably generated due to baroclinic or barotropic instabilities from an unstable boundary current. Also it is accepted that nonlinear eddies are mainly generated in other eastern boundary current systems by instabilities of the near coastal currents [e.g. Chaigenau et al. (2011)]. Therefore the near surface boundary current was investigated. The boundary current off the coast of Mauretania displays a strong seasonality: it is southward directed in boreal winter, northward directed during boreal summer, vanishes during boreal autumn and slowly begin to reverse

and turn southward again during boreal winter. Strongest velocities are recorded in boreal summer. See chapter *2.4 The upper circulation of the tropical northeast Atlantic,* Figure 6 or Figure 27 for more information.

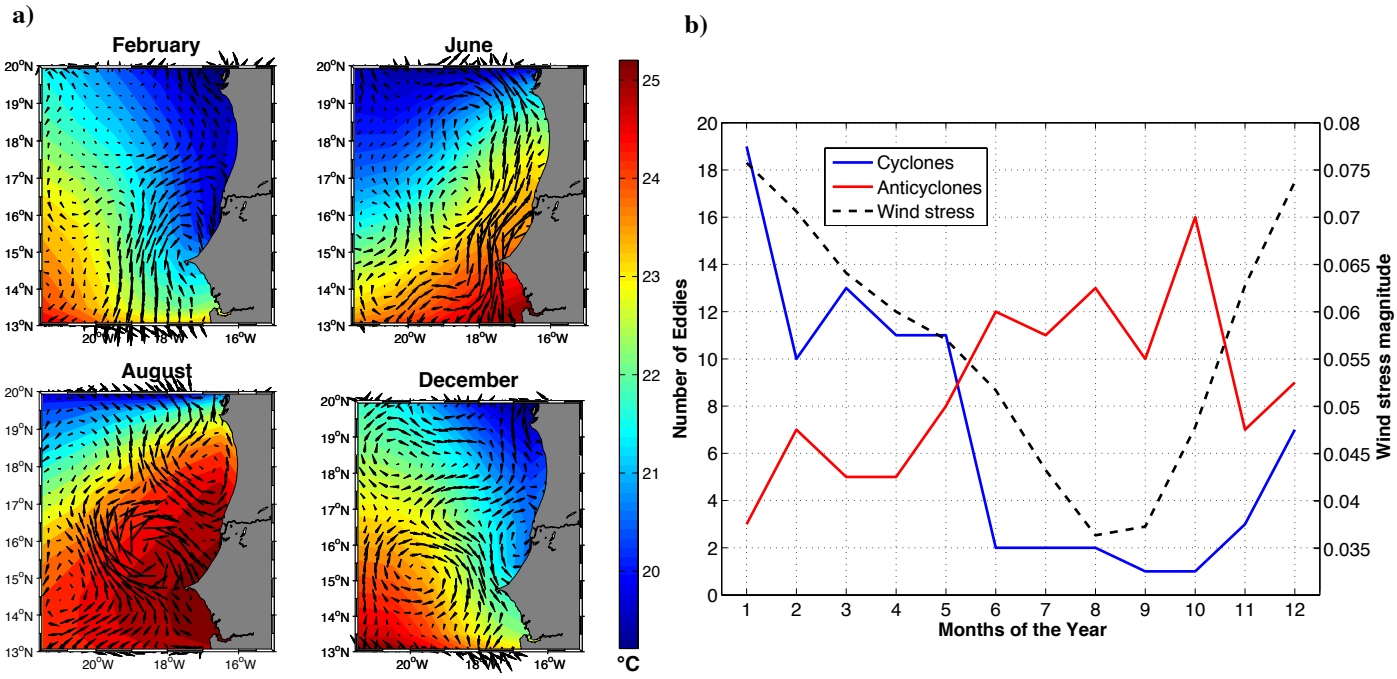

Figure 27: a) Climatology of the SST (color) superimposed is the climatology of geostrophic surface velocities. **b)** Climatology of new detected cyclones (blue) and anticyclones (red) in the coastal area with the climatology of the wind stress magnitude at the position 15°09'N and 17°22'30W, which is slightly north of Cap Vert.

Figure 27a) shows the climatologies of the SST (color) and geostrophic surface velocities (arrows), to show the environmental conditions around the headlands through the year. To draw connections the different climatologies of the generation of anticyclones, cyclones and the wind stress is shown in Figure 27b. The seasonal behaviour of the wind stress and the number of generated cyclones is similar, whereas the anticyclones show a contrary behaviour. Wind stress is highest in January, which is the time of the year the ITCZ is most in the south and the north eastern trade winds are strongest at that location. It is obvious that the source of the reverse of the current in southward direction in January is due to the onset of these strong wind events, which are also responsible for the strong upwelling at the coast during that time. Within the wind events the coastal upwelling reaches its maximum and therefore the UUC has its maximum velocities flowing poleward in depth of ~100m to ~200m at the shelf, for more information see *2.4 The upper circulation of the tropical northeast Atlantic* or Figure 6. These phenomena seem to be in connection with the generation of cyclones. That concludes that the cyclones are generated due to the instabilities from the reverse boundary current or the UUC during winter caused by the onset of strong wind events.

As mentioned previously the generation of anticyclones has contrary seasonal behaviour (red

line) to the generation of cyclones (Figure 22b). The highest amount of anticyclones generated in late summer and October can be attributed to the instabilities of the strong northward boundary current velocities in July, which become unstable in the following months.

The reason for the strong northward velocities, which set in in July is not clear. Knowing is that the ITCZ is furthest north at that time, therefore the southeast winds at the equator are strongest and the equatorial current bands accelerate. One explanation for the strong northward directed velocities near the coast of Mauretania might be that a coastal Rossby wave generated from the strong wind events at the equator is travelling northward. After some time the northward velocities become unstable at the headlands and anticyclones are generated.

The seasonal behaviour of the boundary current and the development of cyclones in January and anticyclones in late boreal summer can also be seen in the single pictures of the following Figure 23. It shows the mean geostrophic surface velocities, calculated from SLA data, plotted as arrows for every month for the year 2000, as an example.

In the first figure the surface velocities from January are shown and southward boundary velocities are detectable near the African coast. Further offshore almost no velocities are visible.

In February the southward boundary current weakened and these instabilities formed a cyclone near Cap Vert. In the next three months of March, April and May no strongly directed surface velocities were detectable. In June a strong northward boundary current set in. By July the current has already become unstable and began to meander. This led to instabilities and the generating of anticyclones in August, September and October. In November the velocities slow down again and have no special direction. In December the onset of stronger south-eastern trade winds began and the surface velocities show a southward component again.

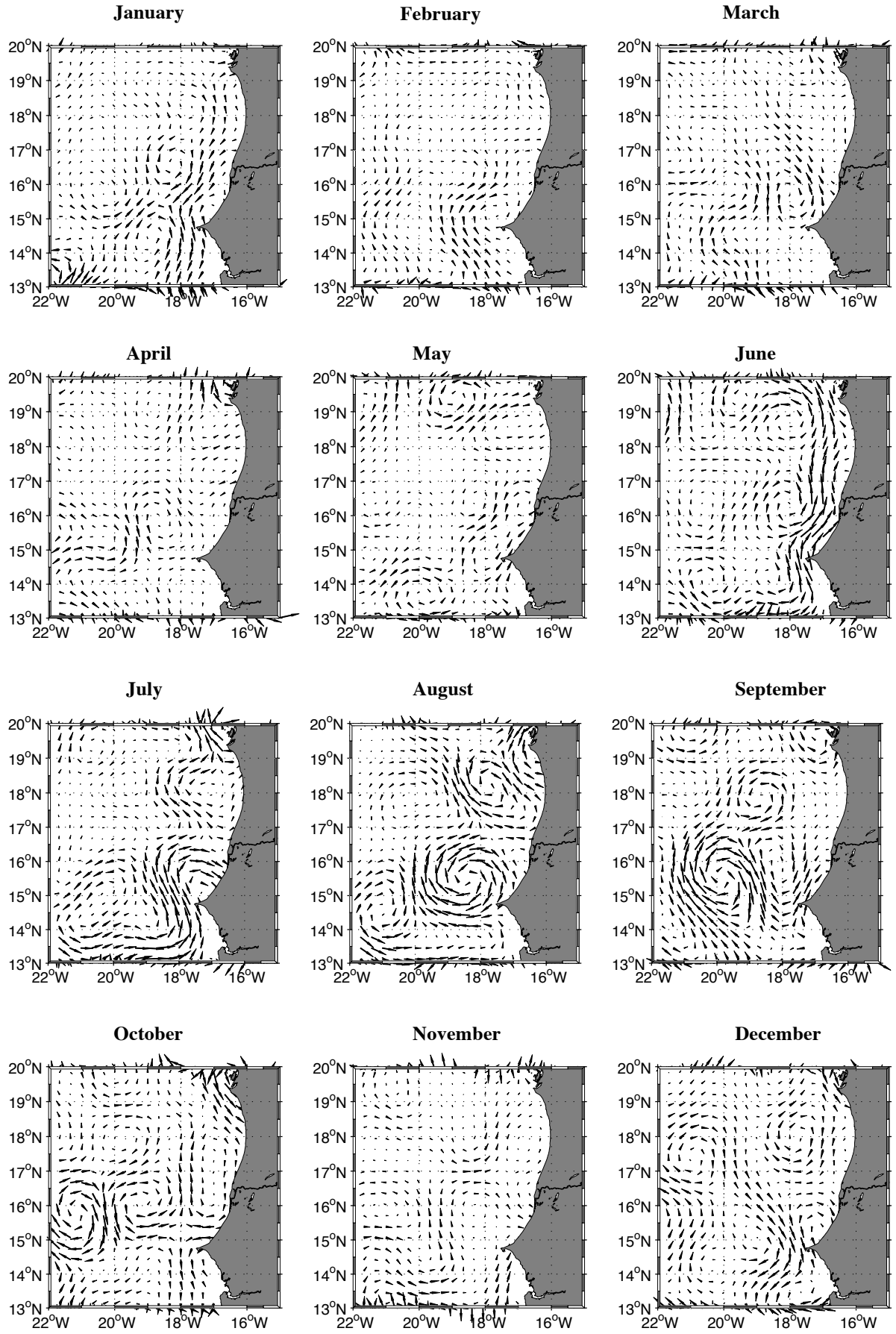

Figure 28: Mean geostrophic velocities from January, February, March, April, May, June, July, August, September, October , November and December exemplary from the year 2000.

It is difficult to say whether barotropic or baroclinic instabilities are the main generating mechanism with regard to instability factors of the boundary current by examining the given datasets. A good approach for further research would be to investigate the instability with regard to a numerical model.

However, after generation at the coast the eddies are observed to travel westward into the open ocean, due to the beta effect. Leaving the boundary region with its stronger boundary current velocities it seems that anticyclones have a southward or equatorwards directed component in their westward movement. Whereas cyclones tend to have a northward or poleward directed component in their westward movement. This different preferences of the meridional deflection for eddies of different polarity is in agreement with other eddy observations, e.g. in the global eddy statistic from Chelton et al. (2007 & 2011). This phenomenon is explainable by the a combined consequence of the beta effect and eddy self advection [Mc Williams (1979), Early et al. (2011)].

6. Summary

Observed single eddy events in the region of the tropical northeast Atlantic existed in length scales between 30km to 110km and time scales of a few days up to nine months. Their vertical velocity structures varied between high and low baroclinic modes and it could be distinguished between eddies, which were surface intensified, and others which had their maximum velocities beneath the surface. The majority of the observed vertical structures were found to be mode water eddies, with a weak SLA signature.

It is shown that eddies lose energy in terms of a decrease in mean vorticity and EKE. At the same time a lowering and decreasing of the maximum azimuthal velocities from a depth of 40 m to 75 m was observed during the lifetime of the ACME 2007. An interesting question for further research might be, if it the sinking of the eddy core is a common phenomenon for eddies in this area, since the deeper eddy core results also in a weaker SLA signature.

In addition a pulsation of the radius and the SLA signature during the lifetime of an eddy was also detected, with a periodicity of ~14 days.

Another result of this study is observed areas where the eddy SLA signature is regularly getting lost. The theory that wind events might hide the SLA signature is an interesting field for further research.

All these phenomena, the fact that most of the eddies are mode water eddies, the fact that the eddy core is sinking during its lifetime and the fact that the eddies seem to pulsate, possible wind events hiding the SLA signature, make the detection and characterising of these eddies with the Eddy-Tracking-Algorithm a very difficult task. The probability of 'loosing' these eddies due to their weak surface signature is highly increased. For the results of the Eddy-Tracking-Algorithm this means an underestimation of the strength of the eddy events, their lifetime and at the same time an overestimation of the number of eddy events. One or a mixture of these problems might have lead to the results of Chelton et al. (2007) or Chelton et al. (2011), who did not find any eddies with a lifetime longer than 3 months in the tropical northeast Atlantic using an automatic Eddy-Tracking-Algorithm. Regarding the given examples of ACME 2007 or ACME 2010, which were observable for a time span of over 9 month, but were also lost and retrieve by the Eddy-Tracking-Algorithm several times, the estimated number from Chelton et al. is not entirely true. The result was achieved due to the fact that the Eddy-Tracking-Algorithm underestimated the lifetime of eddies. The improvement of the autonomous Eddy-Tracking-Algorithms, which are used for studying the mesoscale variability, should be object of further research.

The majority of the observed eddies are topographically generated near the headlands of Senegal and Mauretania by instabilities of the near coastal currents. They all propagate westward due to the β-effect and are found to be nonlinear, meaning their translation velocity is smaller than their rotation velocity. Due to their nonlinearity the eddies are an enclosed system and capture water masses in their cores, transporting water properties from the coast into the offshore ocean. In this area SACW is transported from the upwelling region over the CVFZ into a region where NACW dominates. It is shown that the eddy core suffers almost no lateral mixing with the surrounding water mass on its westward way. The captured water mass contains marine biology consuming the oxygen. Since the mixing is inhibited, the oxygen content in the core of the eddy is strongly decreased during its lifetime. This has been observed several times in a drop below a severe hypoxic level (<20 μmol kg^{-1}) beneath the mixed layer of the eddy at the CVOO mooring [Karstensen et al. (submitted work)].

Besides the known problems the results of the Eddy-tracking-Algorithm, give us some interesting statistics. On average ~17 ±5 eddies per year are produced in the in the upwelling region between Senegal and Mauretania. The production places can be localized from the shape of the coast with its headlands. Most of the eddies are found to be formed near the headland of Cap-Vert and slightly north of it. Another production place is located more north at Cape Nouamghar. The production mechanisms are mainly instabilities of the boundary current due to its seasonality. Due to the effect of the instabilities from a wind induced southward boundary current in boreal winter mainly cyclones are produced, especially in January. On the other hand anticyclones are generated during late boreal summer due to instabilities of a strong northward boundary current. This current is most likely induced by coastal Kelvin waves, which are produced due to strong wind events at the equator during that season.

The overall number of anticyclones produced in one year is higher than the number of yearly produced cyclones. On average 10 ±3 anticyclones and 7 ±3 cyclones were build in the area. Anyhow, the general eddy production activity is with a value of 27% highest in January, the main production month of cyclones. This is due to the fact, that the peak in generated cyclones is much more pronounced, than the one of the anticyclones, which is more smoothly distributed over boreal summer.

The investigation of the different generating mechanism of mesoscale variability near the coast with the help of a numerical model would be an interesting topic for further research.

The different instability terms of the boundary current with regard to e.g. equatorial Kelvin waves, coastal Kelvin waves, the large scale circulation and different wind events could be examined like Liang et al. (2012) did in the eastern Pacific.

After its generation an average anticyclone (cyclone) in the tropical northeast Atlantic travels westward with 3.54 ±1.32 km/d (2.68 ±0.9 km/d) away from the coast into the open ocean. On average all eddies have a radius of 59 ±17.02 km and an average lifetime of 39 ±35 days. The analyses in the area of interest introduced a structure to the unorganised, random pathways of the eddies, as it seems to appear from Figure 1. The eddies follow distinct expansion corridors and on their way the anticyclones (cyclones) experience a meridional deflection towards the equator (pole).

7. References

- W. Alpers, P. Brandt, A. Lazar, D. Dagorne, B. Sow, S. Faye, A. Rubino, P.-M. Poulain and P. Brehmer (2013),
A sub-mesoscale oceanic eddy off the coast of West Africa studied by multi-sensor satellite and surface drifter data and by numerical modeling
Remote Sensing of Enviroment (2012), http://dx.doi.org/10.1016/j.rse.2012.10.032

- Athie, G. and F. Marin (2008),
Cross-equatorial structure and temporal modulation of intraseasonal variability at the surface of the Tropical Atlantic Ocean
Journal of Geophysical Reasearch, Vol. 113

- Böning C. W. and J. Kröger (2005),
Seasonal variability of deep currents in the equatorial Atlantic: a model study
Deep Sea Research Vol. 52, http://dx.doi.org/10.1016/j.dsr.2004.06.015

- Brandt P., G. Caniaux, B. Bourlé, A. Lazar, M. Dengler, A. Funk, V. Hormann, H. Giordani and F. Marin (2010),
Equatorial upper-ocean dynamics and their interaction with the West African monsoon
Atmospheric Science Letters, Vol. 12, 24-30

- Chaigneau, A.,M. Le Texier, G. Eldin, C. Grados and O.Pizarro (2011),
Vertical structure of mesoscale eddies in the eastern South Pacific Ocean: A composite analysis from altimetry and Argo profiling floats
Journal of Geophysical research, 116, C11025, doi:10.1029/2011JC007134

- Chelton D. B., R. A. DeSzoeke, M. G. Schlax, K. el Naggar and N. Siwertz (1998),
Geographical Variability of the First Baroclinic Rossby Radius of Deformation
Journal of Physical Oceanography, Vol. 28, 433-460

- Chelton D. B., M. G. Schlax, R. M. Samelson and R. A. DeSzoeke (2007),
Global observations of large oceanic eddies
Geophysical Research Letters, Vol. 34, L15606, doi:10.1029/2007GL030812

- Chelton D. B., M. G. Schlax and R. M. Samelson (2011),
Global observations of nonlinear mesoscale eddies
Prog. Oceanogr. 91, 167

- Early J., R.M. Samelson and D.B. Chelton (2011),
The Evolution and Propagation of Quasigeostrophic Ocean Eddies
doi:10.1175/2011JP4601.1

- Frankignoul, C. and P. Müller (1979),
Quasigeostrophic response of an infite beta-plane ocean to stochastic forcing by the atmosphere
J. Phys. Ocean, 9, 104-127

- Fischer, J., P. Brandt, M. Dengler, M. Müller und D. Symonds (2003),
Surveying the upper ocean with the ocean surveyor: A new phased array Doppler current profiler
Journal of Atmospheric and Oceanic Technology, 20 (5), S. 742–751

- Foltz G.R, S.A. Grodsky and J.A. Carton (2003),
Seasonal mixed layer heat budget of the tropical Atlantic Ocean
Journal of Geophysical research, 2003

- Ganachaud, A. und C. Wunsch (2000),
Improved estimates of global ocean circulation, heat transport and mixing from hydrographic data
Nature, 408 (6811), S. 453–457

- Gill, A. E., (1982),
Atmosphere-Ocean Dynamics
Academic Press, New York

- Glessmer, M. S., C. Eden und A. Oschlies (2009),
Contribution of oxygen minimum zone waters to the coastal upwelling off Mauritania
Progress in Oceanography, 83 (1-4), S. 143–150

- Grodsky S. A. and J. A. Carton (2002),
Surface drifter pathways originating in the equatorial Atlantic cold tongue
Geophysical Research Letters, DOI: 10.1029/2002GL015788

- Grodsky S. A., J. A. Carton, C. Provost, J. Servain, J. A. Lorenzzetti, and M. J. McPhaden (2005),
Tropical Instability Waves at 0°N, 23°W in the Atlantic: A case study using PIRATA mooring data
Journal of Geophysical Research – Oceans, May 20, 2005

- Gruber N., Z. Lachkar, H. Frenzel, P. Marchesiello, M. Münnich, J. C. McWilliams, T. Nagai and G.-K. Plattner (2011),
Eddy-induced reduction of biological production in eastern boundary upwelling systems
Nature Geoscience DOI: 10.1038/NGEO1273

- Hagen, E., (2001),
Northwest African upwelling scenario
Oceanologica Acta, 24, S. 113–128,

- Holton, J.R., (1979),

An introduction to dynamic meteorology.

2nd ed. Academic Press, New York.

- Isern-Fontanet, J., Garcia-Ladona, E., and Font, J. (2006),
Vortices ofthe Mediterranean Sea: An altimetric perspective.
J. Phys. Oceanogr., 36, 87–103, 2006

- Karstensen J., B. Fiedler, P. Brandt, J. Hahn, T. Kanzow, A. Koertzinger, G. Krahmann. M. Visbek, D. Wallace and R. Zantop (submitted work),
Dead-zone eddies in the tropical North Atlamtic Ocean
Submitted work

- Karstensen, J. und D. Quadfasel (2002),
Formation of southern hemisphere thermocline waters: Water mass conversion and subduction
Journal of Physical Oceanography, 32 (11), S. 3020–3038.

- Leeuwen P. J. (2006),
The Propagation Mechanism of a Vortex on the β Plane
Journal of Physical Oceanography, Vol. 37, pp. 2316-2330, doi:10.1175JPO3107.1

- Liang, J.-H., J. C. McWilliams, J. Kurian, F. Colas, P. Wang, and Y. Uchiyama (2012),
Mesoscale variability in the northeastern tropical Pacific: Forcing mechanisms and eddy properties,
J. Geophys. Res., 117, C07003, doi:10.1029/2012JC008008.

- Luyten, J., J. Pedlosky, and H. M. Stommel (1983),
The ventilated thermocline
J. Phys. Oceanogr. Vol. 13, 292-309.

- McWilliams, J. C., and G. R. Flierl (1979),
On the evolution of isolated, nonlinear vortices,
J. Phys. Oceanogr., 9, 1155–1182.

- Malanotte-Rizzoli P., K. Hedstrom, H. Arango and D.B. Haidvogel (2000),
Water mass pathways between the subtropical and tropical ocean in a climatological simulation of the North Atlantic ocean circulation
Dynamics of Atmosphere and Oceans, Vol. 32, 331-371

- Mittelsteadt E. (1991),
The ocean boundary along the northwest African coast: Circulation and oceanographic properties at the sea surface
Prog. Oceanog. Vol. 26, pp. 304-355, 1999

- Morrow R. and P-Y Le Traon (2007),
15 Years of Satellite Altimetry and mesoscale ocean dynamics
http://earth.esa.int/workshops/venice06/participants/889/paper_889_morrow-v2.pdf

- Okubo, A. (1970),
Horizontal dispersion of floatable particles in the vicinity of velocity singularity such as convergences,
Deep-Sea Res.,17, 445–454, 1970.

- Okumura Y. and S.-P. Xie (2004),
Interaction of the Atlantic Equatorial Cold Tongue and the African Monsoon
American Meteorological Society, Vol. 17

- Pena-Izquierdo J., J. L. Pelegri, M. V. Pastor, P. Castellanos, M.L Eemelianov, M. Gasser, J. Salvador and E. Dominguez (2012),
The continental slope current system between Cape Verde and the Canary Islands
Spanish physical Oceanography, doi: 10.3989/scimar.03607.18C

- Risien, C. M., and D. B. Chelton (2008),
A global climatology of surface wind and wind stress fields from 8 years of QuikSCAT scatterometer data,
J. Phys. Oceanogr., 38, 2379–2413.

- Rossby T., C. Flagg, P. Ortner and C. Hu (2011),
A tale of two eddies: Diagnosing coherent eddies through acoustic remote sensing
Journal of Geophysical research, 116, C12017, doi:10.1029/2011JC007307

-Sangrá P., A. Pascual, A.R. Santana, F. Machin, E. Mason, J.C. McWilliams, J.L.Pelegri, C. Dong, A. Rubio, J. Aristegui, A.M. Diaz, A. Guerra, A. Marrero, M. Auladell (2009),
The CanaryEddyCorridor: A major pathway for long-lived eddies in the subtropical North Atlantic
Elsevier Ltd. doi:10.1016/j.dsr.2009.08.008

- Sangrá, P. Pelegri, J.L. Hernandez-Guerra, A. Arregui,I.,Martin, J.M. Marrero-Diaz, A.,Martinez, A.W., Ratsimandresy, A., R. Santana, (2005) ,
Life history of an anticyclonic eddy
Journal of GeophysicalResearch11,C03021

- Schafstall J. (2010),
Disertation: Turbulente Vermischungsprozesse und Zirkulation im Auftriebsgebiet vor Nordwestafrika

- Schott, F., J. McCreary und G. Johnson, (2004)
Shallow overturning circulations of the tropical-subtropical oceans
In: *Earth's Climate: The Ocean Atmosphere Interaction*, C. Wang, S. Xie und J. Carton, Hg., AGU, Washington, D.C., S. 261–304.

- Souza J.M.A.C., C. de Boyer Montegut and P.Y. Le Traon (2011),
Comparison between three implementations of automatic identification algorithms for the quantification and characterization of mesoscale eddies in the South Atlantic Ocean
Ocean Sci. Discuss., 8, 483-531. 2011 doi:10.5194/osd-8-483-2011

- Stramma, L., P. Brandt, J. Schafstall, F. Schott, J. Fischer und A. Körtzinger (2008),
Oxygen minimum zone in the North Atlantic south and east of the Cape Verde Islands
Journal of Geophysical Research-Oceans, 113 (C4)

- Tomczak, M. (1973),
An investigation into the occurrence and development of cold water patches in the upwelling region off NW Afrika
Meteor-Forschungs-Ergebnisse, A13, S. 1–42.

- Weiss, J. B. (1991),
The dynamics of enstorphy transfer in two dimensional hydrodynamics,
Physica D, 48, 273–294, 1991.

8. Erklärung

Hiermit erkläre ich, Florian Schütte, dass ich die vorliegende Arbeit selbständig und ohne fremde Hilfe angefertigt und keine anderen als die angegebenen Quellen und Hilfsmittel verwendet habe. Die eingereichte schriftliche Fassung der Arbeit entspricht der auf dem elektronischen Speichermedium. (Name der Datei: 898872)

Weiterhin versichere ich, dass diese Arbeit noch nicht als Abschlussarbeit an anderer Stelle vorgelegen hat.

_____

Datum, Unterschrift